

Original Article

Cite this article: Wei W, Lv X-B, and Wang X-D (2021) The granite porphyry hidden in the Shuangjiazishan deposit, southern Great Xing'an Range, NE China: geochronology, isotope geochemistry and tectonic implications. *Geological Magazine* **158**: 995–1009. <https://doi.org/10.1017/S0016756820001065>

Received: 10 November 2019
Revised: 25 August 2020
Accepted: 28 August 2020
First published online: 8 October 2020


Keywords:

granite porphyry; chronology; Great Xing'an Range; Shuangjiazishan; NE China

Author for correspondence: Wei Wei, Emails:

wwei@cug.edu.cn; luxb@cug.edu.cn

The granite porphyry hidden in the Shuangjiazishan deposit, southern Great Xing'an Range, NE China: geochronology, isotope geochemistry and tectonic implications

Wei Wei¹ , Xin-Biao Lv¹ and Xiang-Dong Wang²

¹Institute of Geological Survey, China University of Geosciences, Wuhan 430074, China and ²Wuhan Center of Geological Survey (CGS), Wuhan 430205, China

Abstract

The Shuangjiazishan vein-type Ag-Pb-Zn deposit in the southern Great Xing'an Range (GXR), NE China, is hosted in the slate of the Lower Permian Dashizhai Formation intruded by granite porphyry. In this paper, U-Pb zircon ages and bulk-rock and isotope (Sr, Nd, Pb and Hf) compositions are reported to investigate the derivation, evolution and geodynamic setting of this granite porphyry. It is closely associated with Pb-Zn-Ag mineralization in the southern GXR and contains important geological information relating to regional tectonic evolution. Laser ablation – inductively coupled plasma – mass spectrometry (LA-ICP-MS) zircon U-Pb dating yields an emplacement age of 131 ± 1 Ma for the granite porphyry. Bulk-rock analyses show that the Shuangjiazishan granite porphyry is characterized by high Si, Na and K contents but low Mg and Fe contents, and that the enrichment of Zr, Y and Ga suggests an A-type granite affinity. Most of the studied samples have relatively low $^{87}\text{Sr}/^{86}\text{Sr}$ values (0.70549–0.70558), with positive $\epsilon_{\text{Nd}}(t)$ (0.71–0.88) and $\epsilon_{\text{Hf}}(t)$ (4.9–6.9) values. The Sr–Nd isotope modelling results, in combination with the young T_{DM2} ages of Nd and Hf (850–864 and 668–778 Ma, respectively), reveal that the Shuangjiazishan granite porphyry may be derived from the melting of mantle-derived juvenile component, with minor lower crustal components; this finding is also supported by Pb isotopic compositions. Considering the widespread presence of granitoids with coeval volcanic rocks and regional geology data, we propose that the Shuangjiazishan granite porphyry formed in a post-orogenic extensional environment related to the upwelling of asthenospheric mantle following the closure of the Mongol–Okhotsk Ocean.

1. Introduction

NE China is located in the eastern section of the Central Asian Orogenic Belt (CAOB) (Fig. 1a) and has been jointly influenced by the Palaeo-Asian Ocean, Mongol–Okhotsk Ocean and Palaeo-Pacific tectonic–metallogenic domains (Ouyang *et al.* 2014; Zeng *et al.* 2015; Tang *et al.* 2016; Chen *et al.* 2017; Liu *et al.* 2017). The Palaeo-Asian Ocean was located between the Siberian Craton and the North China Craton (NCC), and the final closure of the Palaeo-Asian Ocean is marked by suturing between the Songliao Block and the Liaoyuan Terrane (Fig. 1b). The closure of the Mongol–Okhotsk Ocean occurred to the NW (current position, F7 in Fig. 1b), and subduction of the Palaeo-Pacific oceanic plate to the east (current position) (Ouyang *et al.* 2015). The distribution of granite in the Great Xing'an Range (GXR), an important part of NE China, is mainly controlled by the different tectonic activities that occurred in different periods. The post-orogenic extension during the Triassic Period followed the closure of the Palaeo-Asian Ocean (Liu *et al.* 2016). The northern Mongol–Okhotsk Ocean between the Siberian Craton and NE China closed during Middle–Late Jurassic time (Kravchinsky *et al.* 2002; Cogné *et al.* 2005), and mass subduction of the southeastern Palaeo-Pacific Plate beneath NE China started during the Early Cretaceous Epoch (Zorin, 1999; Wu *et al.* 2007; Wang *et al.* 2018). Accordingly, it has been reported by previous researchers that the southern GXR is characterized by widespread Jurassic–Cretaceous (Yanshanian) granites and a small amount of Hercynian granitoids (Wu *et al.* 2000, 2005a; Sui *et al.* 2007; Zhang *et al.* 2010), bounded by the Hegenshan–Heihe Suture to the north, the Xilamulun–Changchun Suture to the south and the Nenjiang Fault to the east (Fig. 1b, c). These immense volumes of granitic rocks have mostly been considered A-type granites (Li & Yu, 1993; Sun *et al.* 2000; Jahn *et al.* 2001; Wu *et al.* 2002; Zhang *et al.* 2007; Yang *et al.* 2013). In addition, geochronological and isotopic studies in the southern GXR (Wang *et al.* 2018) have shown that many contemporaneous and A-type granite-related hydrothermal vein-type ore deposits are comparable with those of

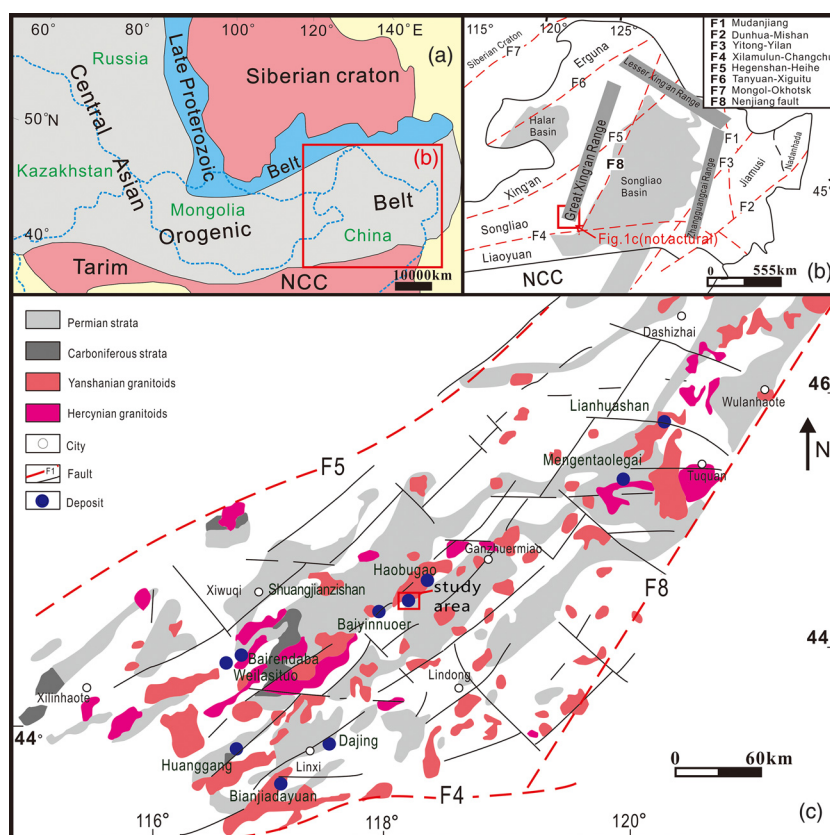


Fig. 1. (Colour online) (a) Location of the Central Asian Orogenic Belt (after Liu *et al.* 2016). (b) Tectonic sketch of NE China (after Wu *et al.* 2011). (c) Regional geological map of the southern Great Xing'an Range (GXR) (after Mei *et al.* 2014).

the adjacent skarn deposits (e.g. the Shuangjianzishan vein-type Ag-Pb-Zn deposit and Haobugao skarn Fe-Zn deposit) and that the magmatism and associated mineralization were coevally generated during the Early Cretaceous Epoch (Zhai *et al.* 2014; Mei *et al.* 2014, 2015; Ruan *et al.* 2015). The origin of these A-type granites therefore has important geological significance and economic potential because of the close association of A-type granites with skarn and epithermal deposits in the southern GXR (Ouyang *et al.* 2013, 2014; Zhai *et al.* 2014; Mei *et al.* 2015; Ruan *et al.* 2015).

The super-large Shuangjianzishan Pb-Zn-Ag deposit, located in southwestern Ganzhuermiao between the Baiyinnuoer and Haobugao deposits (Fig. 1c), is reported to be a typical epithermal vein-type deposit associated with hidden granite porphyry (Wu *et al.* 2013; Liu *et al.* 2016; Gu *et al.* 2017). However, whether the Shuangjianzishan granite porphyry is an A-type granite, and the geodynamic setting and genetic mechanism of this granite, remains ambiguous. Two main possible models are at the centre of this controversy: (1) delamination of the lower crust and lithospheric mantle induced by the subduction of the Palaeo-Pacific Plate (Wu *et al.* 2005b; Wang *et al.* 2006a; Zhang *et al.* 2008; Tian *et al.* 2014; Wang *et al.* 2016b); and (2) post-orogenic lithospheric extension related to the closure of the Mongol–Okhotsk Ocean (Fan *et al.* 2003; Meng, 2003; Ying *et al.* 2010; Wang *et al.* 2018). We consider that it may be feasible to determine which of the two possible models is more likely by investigating the Shuangjianzishan granite porphyry. In this paper, the formation time, evolution and geodynamic significance of Shuangjianzishan granite porphyry (depth greater than 1000 m) and its high affinity with A-type granite are defined by presenting its zircon U–Pb ages and Sr, Nd, Pb and Hf isotopes and whole-rock geochemical data.

2. Geological setting

NE China consists of the Erguna, Xing'an, Songliao, Jiamusi and Nadanhada massifs (Fig. 1b; Fritzell *et al.* 2016; Wang *et al.* 2006b, 2016b). The Erguna Block is of Neoproterozoic age, and Jurassic basalts are widely distributed as dykes (Wu *et al.* 2005c). The oldest basement in the Xing'an Block comprises Palaeozoic amphibolite- to greenschist-facies metamorphic rocks (Miao *et al.* 2007). The underlying basement of the Songliao Basin is composed of Palaeoproterozoic meta-gabbro and meta-granite (Pei *et al.* 2007). The Jiamusi Block contains the Proterozoic Mashan complex and the Early–Late Palaeozoic granitoids (Zhang *et al.* 2010). The Nadanhada Terrane comprises the Raohe complex (a Late Palaeozoic – Jurassic volcano-sedimentary sequence) and undeformed Mesozoic granitoids (Zhang *et al.* 2010; Wu *et al.* 2011). All of these massifs were separated by a series of NE-trending faults (Fig. 1b).

As an important component of NE China, the southern Great Xing'an Range is bounded by the Nenjiang, Hegenshan–Heihe and Xilamulun–Changchun sutures (Fig. 1c). The Palaeo-Asian Ocean, Palaeo-Pacific and Mongol–Okhotsk subductions (Kelty *et al.* 2008; Wang *et al.* 2015; Tang *et al.* 2016; Chen *et al.* 2017; Liu *et al.* 2017) have jointly developed a suite of NE-trending and E–W-trending large-scale faults, which strongly controlled the regional stratigraphic sequence, magmatism and polymetallic mineralization in this region (Fig. 1c). A widespread Permian succession of sedimentary and volcanic rocks makes up much of the GXR, and also the significant ore-bearing strata regionally. Intense magmatic activities produced widespread NE-trending granite bodies, mainly the Yanshanian granitoids, in the southern GXR (Fig. 1c). Wu *et al.* (2003) showed that Mesozoic volcanic rocks and granites in the southern GXR have

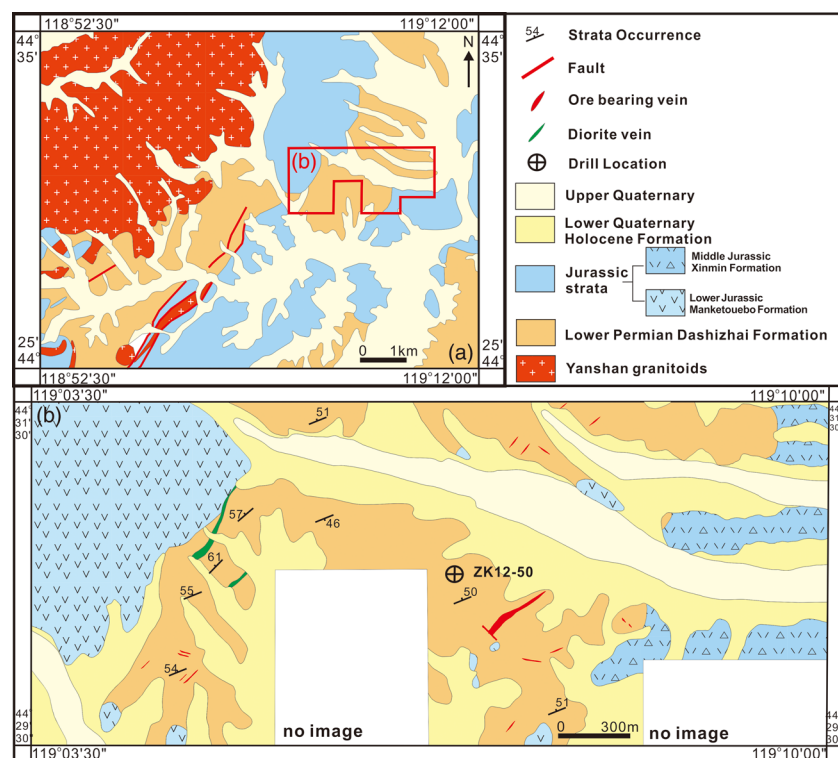


Fig. 2. (Colour online) (a) Geological map of the Shuangjianzishan Pb-Zn-Ag deposit (after Liu *et al.* 2016). (b) Large-scale geological map of the Shuangjianzishan mining area.

low initial $^{87}\text{Sr}/^{86}\text{Sr}$ ratios (0.7045 ± 0.0015), positive $\epsilon_{\text{Nd}}(t)$ values (+1.3 to +2.8) and young Sm-Nd model ages (720–840 Ma). Liu *et al.* (2020) reported that the Wulanba granite in the southern GXR originated from partial melting of juvenile crust derived from the depleted mantle with a minor input of old crust. However, Tang *et al.* (2020) suggested that upper Mesozoic volcanic rocks of the GXR were derived from the partial melting of a mantle wedge that was modified by previously subducted slab-derived fluids, and that the magma was likely introduced with limited crustal contamination. Ouyang *et al.* (2015) identified three magmatic stages of the Mesozoic granitoids that occurred during 255–220 Ma, 184–160 Ma and 155–120 Ma. The intrusive activities peaked during late Mesozoic time (155–120 Ma) and were accompanied by large-scale mineralization. For example, the mineralized Huanggang granite has an age of 135–137 Ma (Mei *et al.* 2014; Zhai *et al.* 2014), the mineralized Baiyinnuoer granite has an age of 135–139 Ma (Jiang *et al.* 2011; Shu *et al.* 2013), the mineralized Haobugao granite has an age of 138–139 Ma (Wang *et al.* 2018) and the mineralized Weilasisuo granite has an age of 133–136 Ma (Pan *et al.* 2009; Zhai *et al.* 2016). The magmatic and mineralizing activity at Shuangjianzishan has been dated at 133–136 Ma (Zhai *et al.* 2020). Several studies of the Shuangjianzishan deposit have addressed the ore deposit geology (Kuang *et al.* 2014), mineralogy (Wu *et al.* 2014), whole-rock geochemistry (Liu *et al.* 2016; Gu *et al.* 2017), magmatic rock and ore geochronology (Wu *et al.* 2013; Liu *et al.* 2016; Ouyang *et al.* 2016; Wang *et al.* 2016a; Wang *et al.* 2018; Zhang, 2018; Zhai *et al.* 2020) and S-Pb isotope geochemistry (Jiang *et al.* 2017; Wang *et al.* 2018). However, questions related to the petrogenesis and the tectonic setting of the Shuangjianzishan granite porphyry remain unresolved. For example, Liu *et al.* (2016) suggested that the porphyritic granodiorite is interpreted as being adakitic and related to the subduction of the Palaeo-Pacific oceanic plate, whereas Gu *et al.* (2017) proposed that granite porphyry formed

in a post-orogenic extensional environment related to the upwelling of asthenospheric mantle due to the deep break of the subducting plate of Mongolia–Okhotsk.

The Shuangjianzishan Pb-Zn-Ag deposit is located in the central part of the Songliao Block (Fig. 1c), which mainly consists of the Upper Jurassic Manketouebo Formation, the Middle Jurassic Xinmin Formation, the Lower Permian Dashizhai Formation and the Quaternary Holocene Formation (Fig. 2b). The Dashizhai Formation comprises tuffaceous and silty slate, and the southeastern Xinmin Formation consists of a suite of volcanoclastic rocks. The northwestern Manketouebo Formation is composed of pyroclastic rocks, felsic lava and andesite. The zircon U-Pb ages of the Manketouebo Formation volcanic rocks are 150–160 Ma (Yang *et al.* 2012). Quaternary sediments, located in the valleys, mainly consist of proluvial and alluvial materials. A large amount of Yanshanian granites are distributed in the northwestern periphery of the mining area (Fig. 2a). An unexposed granite porphyry was discovered by drilling exploration (ZK12-37 in Zhai *et al.* 2020; ZK12-50 in Gu *et al.* 2017). Since the discovery of the Shuangjianzishan deposit, several studies on the geochronology have been completed (Table 1). There are three magmatic periods described by the Shuangjianzishan deposit (254–239 Ma, 169–159 Ma and 135–128 Ma) and there is no final consensus on the age of the granite porphyry. For example, Ouyang *et al.* (2016) consider that U-Pb zircon ages of the granite porphyry are 159 ± 2 Ma. However, most studies suggested that the age of granite porphyry is c. 130 Ma (Liu *et al.* 2016; Wang *et al.* 2016a; Gu *et al.* 2017; Zhai *et al.* 2020).

3. Core and sample descriptions

Zhai *et al.* (2020) subdivided the granite porphyry into lower coarse-grained facies and upper fine-grained facies, and Gu *et al.* (2017) described the mineral composition of the granite hand specimens. According to our observations, the granite porphyry was found in

Table 1. Ages of magmatism in Shuangjianzishan deposit, all determined by zircon U–Pb dating

Sample details	Age (Ma)	References
Weakly Mo-mineralized granite porphyry	134 ± 1	Zhai <i>et al.</i> (2020)
Diorite–granodiorite dykes	250 ± 2	Zhai <i>et al.</i> (2020)
Dacite	134 ± 1	Zhai <i>et al.</i> (2020)
Ore-bearing prophyritic monzogranite	252–254	Liu <i>et al.</i> (2016)
Rhyolitic crystal–vitric ignimbrite	169 ± 3	Liu <i>et al.</i> (2016)
Altered prophyritic granodiorite	130 ± 6	Liu <i>et al.</i> (2016)
Granite porphyry	159 ± 2	Ouyang <i>et al.</i> (2016)
Granite porphyry	133 ± 1	Gu <i>et al.</i> (2017)
Granite porphyry	131 ± 1	Wang <i>et al.</i> (2018)
Biotite granite	134 ± 2	Zhang <i>et al.</i> (2018)
Syenogranite	128 ± 2	Zhang <i>et al.</i> (2018)
Granite porphyry	135 ± 2	Zhang <i>et al.</i> (2018)
Diorite porphyrite	239–246	Wang <i>et al.</i> (2016a)
Diorite porphyrite	249 ± 2	Cui (2015)
Granite in the north of the mining area	134 ± 1	Wu <i>et al.</i> (2014)
Quartz porphyry	239 ± 1	Wu <i>et al.</i> (2014)

the core of drill hole ZK12-50 from a depth of 1011 m to the bottom at 1023 m, and presents uniform coarse-grained facies without facies change at depth. The granite porphyry is in intrusive contact with the Lower Permian Dashizhai Formation and the contact is an intrusive breccia, with xenoliths of Permian slate within the granite. The main alteration in the granite near the contact zone is pyritization (at 1011 m), and the overlying slates have undergone strong chloritic and silicic alteration (from 967 to 952 m) and contain numerous Pb–Zn veins (Fig. 3). From the granite porphyry to the country rock, the alteration varies from pyritization, chloritic to silicic alteration. Under the influence of the magmatic–hydrothermal activity, abundant breccias cemented by minor quartz–calcite occur in the Permian slate, and the ore bodies are lenticular ore-bearing veinlets (Fig. 3). The number of samples is limited as the core column was badly damaged. Nine rock samples from ZK12-50, collected from 1011–1023 m depths at an interval of about 1 m, were analysed for their zircon U–Pb dates and whole-rock and isotope compositions (Table 2). The granite porphyry is red and has a porphyritic texture (Fig. 4a). The phenocrysts are euhedral plagioclase (15–20 vol%), subhedral K-feldspar (10–15 vol%) and subhedral quartz (20–25 vol%) (Fig. 4b, d, e). The dark minerals observed in hand specimens are mainly flake biotite (> 10 vol%). The matrix (30–35 vol%) consists of quartz, plagioclase and K-feldspar with minor hornblende and accessory minerals (< 2 vol%) including rutile, pyrite, zircon and apatite (Fig. 4f). The plagioclase is partially altered to sericite, and the biotite is partially altered to chlorite (Fig. 4c).

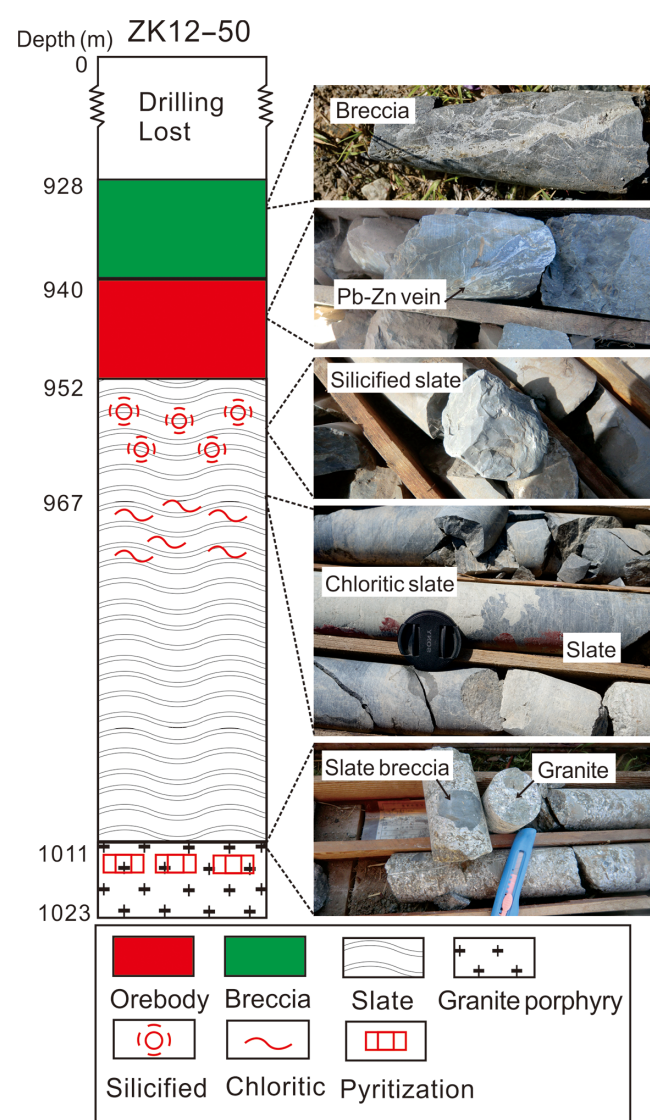
4. Analytical methods

4.a. Zircon U–Pb dating

A total of 21 zircon grains in three samples from drill hole ZK12-50 (depth, 1020 m) were separated using conventional heavy liquid and magnetic techniques and mounted in epoxy blocks. These blocks were then polished to obtain an even surface before analysis by laser

Table 2. Sample collection in Shuangjianzishan deposit, all coarse-grained granite

Sample	Depth (m)	Analytical methods
ZK12-50-1	1012	Whole-rock analyses
50-1	1013.5	Sr–Nd–Pb isotopic analyses
ZK 50-1	1014.5	U–Pb dating and Hf isotopic analyses
ZK12-50-2	1015	Whole-rock analyses
50-2	1016.5	Sr–Nd–Pb isotopic analyses
ZK 50-2	1017	U–Pb dating and Hf isotopic analyses
ZK12-50-3	1018	Whole-rock analyses
50-3	1019.5	Sr–Nd–Pb isotopic analyses
ZK 50-3	1021	U–Pb dating and Hf isotopic analyses

**Fig. 3.** (Colour online) Simplified drill columnar section and photographs of intrusive contact relation.

ablation – inductively coupled plasma – mass spectrometry (LA–ICP–MS). All the zircons were documented via transmitted and reflected light micrographs and cathodoluminescence (CL)

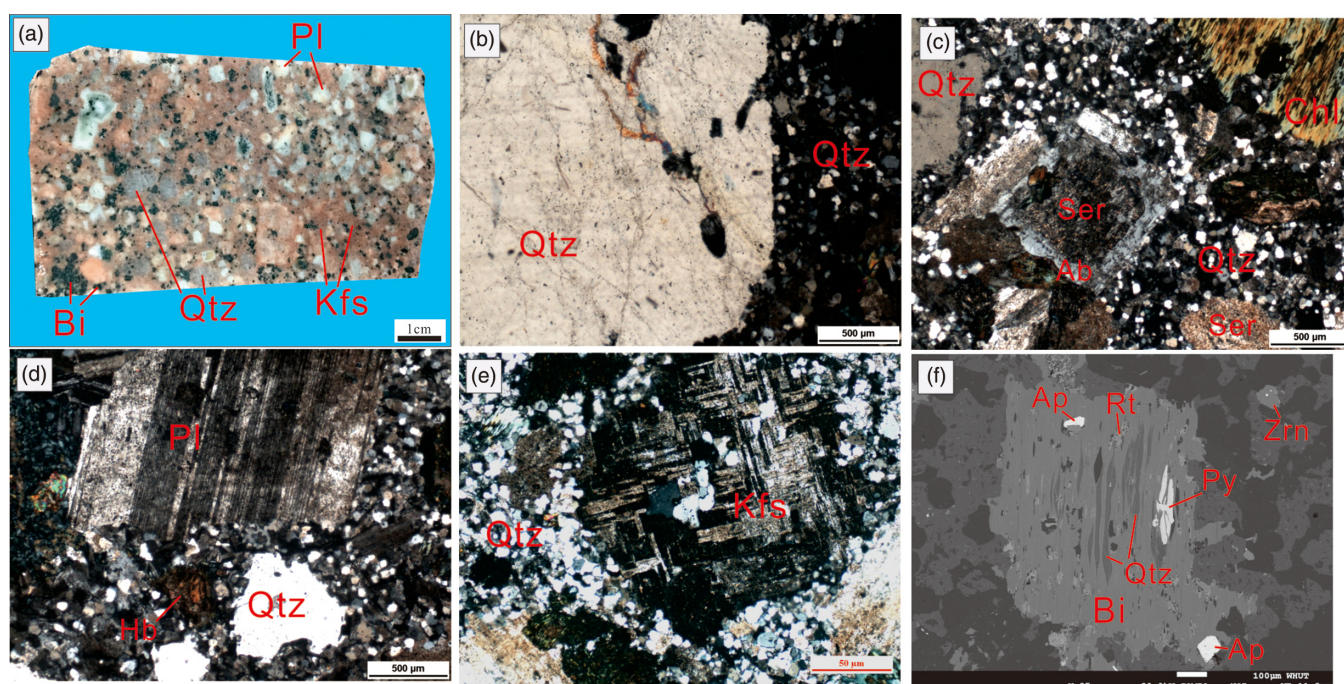


Fig. 4. (Colour online) Hand-specimen photograph, photomicrographs and back-scatter electron image for the Shuangjianzishan granite porphyry: (a) porphyritic texture; (b) quartz phenocryst and matrix quartz; (c) sericite and chlorite alteration; (d) plagioclase phenocryst; (e) K-feldspar phenocryst; and (f) biotite and accessory minerals. Pl – plagioclase; Bi – biotite; Qtz – quartz; Kfs – K-feldspar; Ser – sericite; Ab – albite; Chl – chlorite; Hb – hornblende; Ap – apatite; Zrn – zircon; Py – pyrite; Rt – rutile.

images to reveal their internal structures. These procedures were performed at the State Key Laboratory of Geological Processes and Mineral Resources (GPMR), China University of Geosciences (Wuhan). Zircon U-Th-Pb measurements were carried out under a 32- μm diameter laser beam at the GPMR, and a Geo Las 2005 System was used. An Agilent 7700a ICP-MS instrument was employed to acquire ion-signal intensities with a 193-nm Ar-F excimer laser and a homogenizing, imaging optical system (Micro Las, Göttingen, Germany). A detailed description of the instrumentation and analytical accuracy can be found in Liu *et al.* (2008, 2010). Concordia diagrams were generated and weighted mean calculations were performed using Isoplot/Ex_ver3 (Ludwig, 2003).

4.b. Whole-rock geochemical analyses

Because the rock lithology is relatively uniform without obvious dark enclaves, the sample set is enough when combined with previous studies of the congenetic granites. Three whole-rock samples were crushed and powdered in an agate mill to *c.* 200 mesh. Major-element analyses were carried out at ALS Chemex (Guangzhou) Co., Ltd. by spectrofluorimetry with relative analytical errors of < 5%. The samples created for trace-element analyses were from the same set as for major-element analysis, and digested by HF+HNO₃ in Teflon bombs and analysed with an Agilent 7500a ICP-MS at the GPMR. The detailed sample-digesting procedure for ICP-MS analyses and the analytical precision and accuracy of the trace-element analyses are as described by Liu *et al.* (2008).

4.c. Sr-Nd-Pb and Hf isotopic analyses

Three isotope samples were crushed and powdered in an agate mill to *c.* 200 mesh. Sr and Nd isotopic analyses were carried out via a Micromass Isoprobe multicollector (MC) ICP-MS at the Guangzhou Institute of Geochemistry, Chinese Academy of

Sciences (GIGCAS); the analytical procedures regarding the Sr and Nd isotopes are described in detail by Wei *et al.* (2002) and Li *et al.* (2004). The chemical separation of Sr and Nd was performed via a method similar to the methods described by Li & McCulloch (1998) and Xu *et al.* (2002). Sample powders (50–100 mg) were digested with distilled HF-HNO₃ in screw-top PFA beakers at 120°C for 15 days. Sr and rare earth elements (REEs) were then separated using cation columns, followed by the separation of Nd from the REE fraction using di-2-ethylhexyl phosphoric acid (HDEHP) columns. The ⁸⁷Sr/⁸⁶Sr value of the NBS987 standard and ¹⁴³Nd/¹⁴⁴Nd value of the JNdi-1 standard were 0.710288 ± 28 (2 σ) and 0.512109 ± 12 (2 σ), respectively; all the measured ¹⁴³Nd/¹⁴⁴Nd and ⁸⁷Sr/⁸⁶Sr values were corrected to ¹⁴³Nd/¹⁴⁴Nd = 0.7219 and ⁸⁷Sr/⁸⁶Sr = 0.1194, respectively. Pb isotopic compositions were measured by thermal ionization mass spectrometry (TIMS) using a procedure similar to that described by Xu & Castillo (2004). Pb isotopic ratios were corrected for fractionation using replicate analyses of the standard NBS 981. *In situ* Hf isotopic analyses on the same set of zircons were conducted using a Neptune Plus MC-ICP-MS equipped with a Geolas-2005 193-nm Ar-F excimer laser, also at the GPMR. A laser repetition rate of 10 Hz at 100 mJ was used with a spot size of 44 μm . Details of the analytical technique are described by Hu *et al.* (2012).

5. Results

5.a. Zircon U-Pb geochronology

The CL images of selected zircons are shown in Figure 5. The LA-ICP-MS zircon U-Pb analytical data are summarized in Table 3 and illustrated in the concordia diagram (Fig. 6). The zircon grains from the granite are grey, prismatic and euhedral with oscillatory zoning, showing typical magmatic zircons. Most of these grains have high Th/U ratios ranging from 0.34 to 2.10

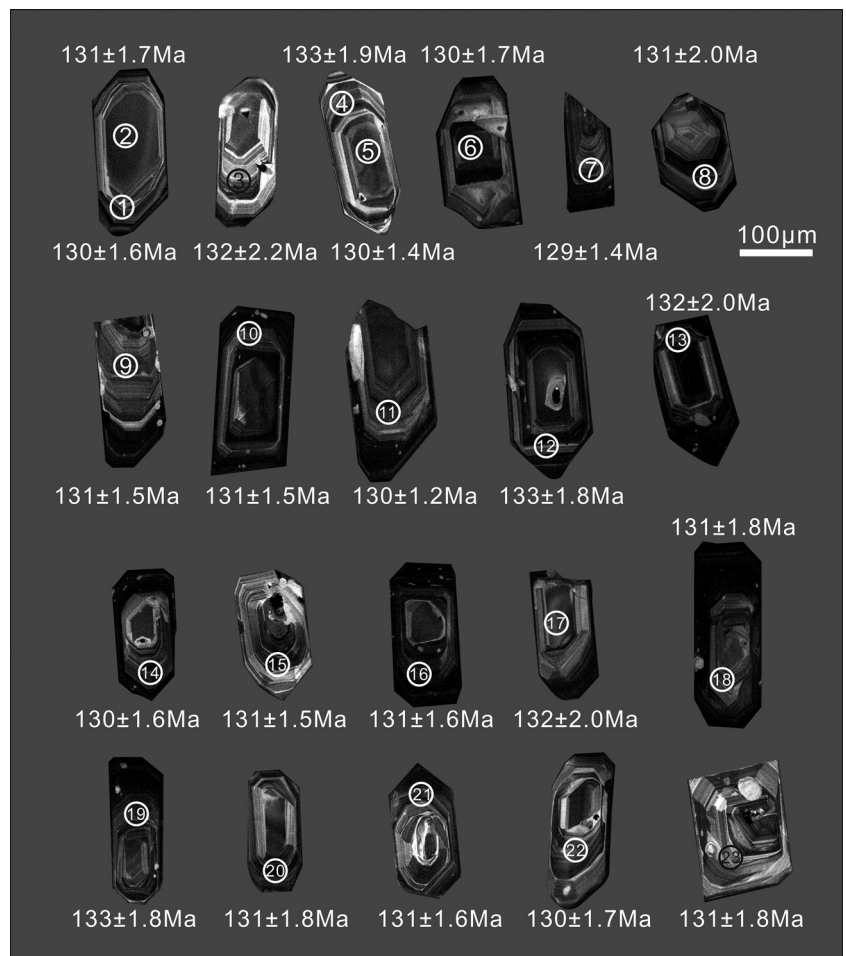


Fig. 5. Representative cathodoluminescence (CL) images of zircons from the Shuangjianzishan granite porphyry. Numbers and ages on zircon grains are the analysed spots in Table 3.

(Table 4), which supports their magmatic origin (Pupin, 1980; Koschek, 1993). A total of 23 analyses from 21 grains yielded concordant results with a weighted mean $^{206}\text{Pb}/^{238}\text{U}$ age of 131 ± 1 Ma (mean square weighted deviation (MSWD) = 0.46, $n = 23$) (Fig. 6), which is interpreted as the crystallization age of the Shuangjianzishan granite porphyry.

5.b. Major- and trace-element geochemistry

The major- and trace-element abundances of three samples are provided in Table 4. All the samples have relatively high concentrations of SiO_2 (69.63–70.32 wt%), Na_2O (4.37–4.38 wt%) and K_2O (3.92–4.29 wt%), with $\text{K}_2\text{O}/\text{Na}_2\text{O}$ ratios of 0.90–0.98, indicating their high-K calc-alkaline composition (Fig. 7a; Peccerillo & Taylor, 1976). The granite porphyry is metaluminous and weakly peraluminous with A/CNK (molar ratio of $\text{Al}_2\text{O}_3/(\text{CaO} + \text{Na}_2\text{O} + \text{K}_2\text{O})$) and A/NK ratios ranging over 0.98–1.01 and 1.21–1.24, respectively (Fig. 7b; Maniar & Piccoli, 1989).

The granite porphyry exhibits moderate REE contents ranging from 151.61 to 156.41 ppm, is enriched in light REEs (LREEs) and depleted in heavy REE (HREEs), has $(\text{La}/\text{Yb})_N$ ratios of 3.16–8.93 and has significant negative Eu anomalies ($\text{Eu}/\text{Eu}^* = 0.37\text{--}0.40$) (Table 4). These samples are rich in large-ion lithophile elements (LILE), but depleted in high-field-strength elements (HFSE), displaying strong negative

anomalies of Ba, Sr, P and Ti (Fig. 7c, d). These features imply the occurrence of apatite and ilmenite fractional crystallization or the presence of residual apatite and ilmenite minerals in the magma source, and the high Rb concentrations (208–220 ppm) suggest that the Shuangjianzishan granite porphyry may have undergone high crystal fractionation (Fig. 7d).

5.c. Sr-Nd-Pb isotopes

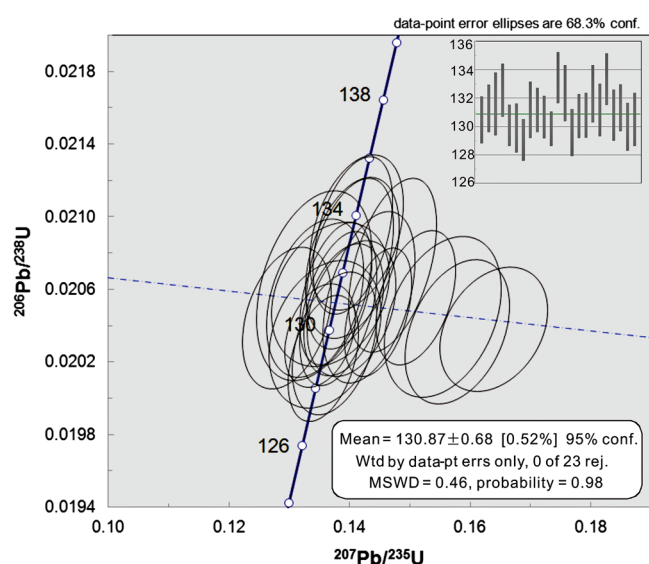
Three samples were analysed for Sr-Nd-Pb isotopic compositions, and the results are presented in Tables 5 and 6. The Shuangjianzishan granite porphyry samples show low $(^{87}\text{Sr}/^{86}\text{Sr})_t$ values of 0.7055–0.7056 and positive $\epsilon_{\text{Nd}}(t)$ values of 0.71–0.88 (Table 5). The two-stage Nd model ages ($T_{\text{DM}2}$) of the Shuangjianzishan granite porphyry are 850–864 Ma. Meanwhile, the Shuangjianzishan granite porphyry samples are characterized by high radiogenic Pb isotope ratios with $(^{206}\text{Pb}/^{204}\text{Pb})_t = 18.12\text{--}18.25$, $(^{207}\text{Pb}/^{204}\text{Pb})_t = 15.52\text{--}15.53$ and $(^{208}\text{Pb}/^{204}\text{Pb})_t = 38.00\text{--}38.11$ (Table 6).

5.d. Zircon Hf isotopic composition

The *in situ* Hf isotopic analysis results of the zircons from the Shuangjianzishan granite porphyry are listed in Table 7. A total of 15 spots of zircon grains obtained from sample ZK12-50 were measured, giving initial $^{176}\text{Hf}/^{177}\text{Hf}$ ratios ranging from 0.282833 to 0.282888 with corresponding $\epsilon_{\text{Hf}}(t)$ values of 4.9–6.9. The $f_{\text{Lu/Hf}}$

Table 3. LA-ICP-MS zircon U–Pb Shuangjiazishan granite porphyry data

Sample or spot	²³² Th (ppm)	²³⁸ U (ppm)	Th/U	²⁰⁷ Pb/ ²³⁵ U	1σ (%)	²⁰⁶ Pb/ ²³⁸ U	1σ (%)	²⁰⁷ Pb/ ²⁰⁶ Pb	1σ (%)	²⁰⁷ Pb/ ²³⁵ U time (Ma)	1σ	²⁰⁶ Pb/ ²³⁸ U time (Ma)	1σ
SJ-1	551	1215	0.45	0.12965	0.00482	0.02044	0.00026	0.0461	0.0017	124	4	130	2
SJ-2	495	907	0.55	0.13693	0.00646	0.02058	0.00026	0.0491	0.0025	130	6	131	2
SJ-3	307	760	0.40	0.13422	0.00632	0.02062	0.00035	0.0478	0.0023	128	6	132	2
SJ-4	647	1407	0.46	0.14051	0.00510	0.02078	0.00029	0.0497	0.0020	133	5	133	2
SJ-5	1146	3003	0.38	0.16403	0.00592	0.02038	0.00023	0.0574	0.0019	154	5	130	1
SJ-6	489	1058	0.46	0.13601	0.00615	0.02036	0.00027	0.0488	0.0023	129	6	130	2
SJ-7	866	2166	0.40	0.13569	0.00390	0.02022	0.00023	0.0486	0.0015	129	3	129	1
SJ-8	716	1889	0.38	0.14329	0.00501	0.02056	0.00031	0.0507	0.0018	136	4	131	2
SJ-9	587	1697	0.35	0.15101	0.00436	0.02056	0.00024	0.0531	0.0016	143	4	131	2
SJ-10	968	2574	0.38	0.14477	0.00369	0.02048	0.00023	0.0509	0.0013	137	3	131	1
SJ-11	795	2526	0.31	0.13514	0.00386	0.02035	0.00019	0.0478	0.0014	129	3	130	1
SJ-12	563	1316	0.43	0.14124	0.00513	0.02092	0.00028	0.0493	0.0020	134	5	133	2
SJ-13	685	1711	0.40	0.14011	0.00477	0.02074	0.00031	0.0487	0.0016	133	4	132	2
SJ-14	917	1868	0.49	0.13754	0.00463	0.02030	0.00026	0.0490	0.0017	131	4	130	2
SJ-15	889	1735	0.51	0.13906	0.00436	0.02049	0.00024	0.0489	0.0016	132	4	131	2
SJ-16	726	2145	0.34	0.14038	0.00485	0.02050	0.00025	0.0493	0.0017	133	4	131	2
SJ-17	1552	2132	0.73	0.14725	0.00482	0.02074	0.00032	0.0515	0.0016	139	4	132	2
SJ-18	364	1181	0.31	0.13433	0.00535	0.02056	0.00029	0.0472	0.0019	128	5	131	2
SJ-19	706	1973	0.36	0.14056	0.00436	0.02090	0.00028	0.0486	0.0015	134	4	133	2
SJ-20	1257	1925	0.65	0.13820	0.00423	0.02050	0.00028	0.0491	0.0016	131	4	131	2
SJ-21	922	2096	0.44	0.13777	0.00399	0.02058	0.00026	0.0489	0.0016	131	4	131	2
SJ-22	575	1177	0.49	0.15797	0.00571	0.02037	0.00026	0.0568	0.0022	149	5	130	2
SJ-23	322	788	0.41	0.15557	0.00640	0.02045	0.00029	0.0556	0.0023	147	6	131	2

**Fig. 6.** (Colour online) Zircon U–Pb concordia diagrams for the Shuangjiazishan granite porphyry. The concordia age, mean age and mean square weighted deviation (MSWD) are shown in each figure.

values range over -0.98 to -0.96 , which are much lower than the $f_{LW/Hf}$ values of oceanic crust and continental upper crust (-0.34

and -0.72 , respectively) (Amelin *et al.* 2000). The two-stage model ages (T_{DM2}) vary from 668 to 778 Ma (Table 7).

6. Discussion

6.a. Late Jurassic – Early Cretaceous granitic magmatism

The results of the zircon LA-ICP-MS U–Pb dating at Shuangjiazishan yield a diagenetic age of 131 ± 1 Ma for the granite porphyry, consistent with the age of 131–135 Ma presented in previous reports (Table 1). Wu *et al.* (2013) reported a sphalerite Rb–Sr isochron age of 133 ± 4 Ma, and Zhai *et al.* (2020) dated a molybdenite Re–Os age of 134.9 ± 3.4 Ma. The magmatic events that occurred slightly before 130 Ma are therefore coeval with the Pb–Zn–Ag mineralization. In addition, this paper does not contradict the views of Liu *et al.* (2016), Ouyang *et al.* (2016) or Wang *et al.* (2016a) on the possibility of superimposed mineralization via two periods of mineralization (at c. 165 Ma and c. 130 Ma). However, the major mineralization of the Shuangjiazishan deposit was triggered by the granite porphyry intrusion, which occurred over a short interval during the Early Cretaceous Epoch.

6.b. Petrogenesis and evolution of the Shuangjiazishan granite porphyry

Granitoids have traditionally been classified as I-, S- and A-types based on chemical and mineralogical compositions (Chappell &

Table 4. Major- (wt%) and trace-element (ppm) contents of the Shuangjianzishan granite porphyry

	ZK12-50-1	ZK12-50-2	ZK12-50-3
SiO ₂	70.32	70.19	69.63
TiO ₂	0.33	0.35	0.36
Al ₂ O ₃	14.29	14.08	14.42
Fe ₂ O ₃	2.86	2.99	3.12
MnO	0.05	0.05	0.06
MgO	0.58	0.63	0.64
CaO	1.47	1.68	1.45
Na ₂ O	4.38	4.37	4.38
K ₂ O	4.29	3.92	4.10
P ₂ O ₅	0.08	0.09	0.09
LOI	1.12	1.06	1.09
Total	99.77	99.41	99.34
A/CNK	0.98	0.97	1.01
A/NK	1.20	1.23	1.24
Rb	214.00	208.00	220.00
Ba	534.00	465.00	555.00
Th	22.00	21.90	20.40
U	8.20	8.15	7.34
Ta	2.30	1.80	1.70
Nb	12.90	13.10	14.00
Sr	271.00	273.00	275.00
Nd	25.20	25.90	25.00
Zr	167.00	188.00	194.00
Hf	5.60	5.80	6.10
La	32.20	31.30	30.00
Ce	66.80	66.80	64.80
Pr	7.03	7.17	6.92
Sm	5.27	5.55	5.54
Eu	0.66	0.65	0.70
Ga	22.60	24.50	24.50
Gd	4.70	5.03	5.09
Tb	0.79	0.86	0.86
Dy	4.76	4.96	4.97
Ho	0.99	1.01	0.96
Er	2.70	3.02	2.83
Tm	0.44	0.45	0.47
Yb	3.02	3.23	3.02
Lu	0.45	0.48	0.45
Y	30.70	32.60	31.80
Eu/Eu*	0.40	0.37	0.40
(La/Yb) _N	7.65	6.95	7.13
ΣREE	155.01	156.41	151.61

White 1974, 1992; Hineab *et al.* 1978; Whalen *et al.* 1987). As the emplacement ages of the regional Yanshanian granite and the adjacent Haobugao granite are mainly concentrated within Early Cretaceous time, plotting the chemical composition of these granites is useful for comparison of the Shuangjianzishan granite porphyry with the pervasive Early Cretaceous magmatism. Samples from the Shuangjianzishan granite porphyry are metaluminous to peraluminous (Fig. 7b) and plot within the high-K calc-alkaline series (Fig. 7a), consistent with the adjacent Haobugao granite and most of the Yanshanian granite. Chondrite-normalized REE patterns show that the samples are obviously enriched in LREEs, depleted in HREEs, and have strongly negative Eu anomalies (Fig. 7c). Compared with primitive mantle, the Shuangjianzishan granite porphyry is enriched in Zr, Hf, Rb, Th and U and depleted in Ba, Sr, P and Ti (Fig. 7d), which is similar to typical A-type granite (Li *et al.* 2014). S-type granites always contain more Al than that required to form feldspar, and the excess Al is hosted in Al-rich biotite, generally accompanied by more Al-rich minerals such as cordierite or muscovite (Chappell, 1984; Chappell *et al.* 2012). However, the Shuangjianzishan granite porphyry has a low biotite content (Fig. 4f). In addition, the measured A/CNK values are no less than 1.1 (Fig. 7b), indicating that the samples are A-type or I-type granites, not S-type granites (Chappell & White, 1992; Chappell, 1999).

A-type granites are widely distributed and closely associated with I-type granites in NE China. Due to the uncertainty and diversity of geological processes and the geochemical behaviour of elements, many researchers (Tian *et al.* 2014) have found that it is difficult to distinguish the A- and I-types in the GXR based on only the discrimination diagrams. In addition, the A-type granites have the same Sr–Nd isotopic characteristics as the I-type granites, indicating that they are derived from the same source (Wu *et al.* 2002; Wang *et al.* 2018). A-type granites are usually formed under conditions of high temperature and low pressure (Collins *et al.* 1982; Clemens *et al.* 1986), and therefore generally contain relatively high-temperature anhydrous minerals, such as pyroxene, fayalite and interstitial biotite (Collins *et al.* 1982; Whalen *et al.* 1987; Eby, 1992) and are enriched in HFSEs such as Zr, Nb, Y, REE and Ga. Wu *et al.* (2002) found that A-type granites in NE China usually contain alkali mafic minerals, such as sodic pyroxene, or contain annite and Fe-rich calcic amphibole. From microscopic observation, many biotite and hornblende grains were found in the Shuangjianzishan granite porphyry (Fig. 4a, d). In the diagrams of K₂O+Na₂O, FeO*/MgO, Nb versus Ga/Al, all the Shuangjianzishan granite porphyry and regional granite samples plot in the A-type field, suggesting that they are A-type granites (Fig. 8a–c). Moreover, in the Nb–Y–Ce diagram (Fig. 8d), all the granite samples plot in the A₂ group, suggesting a post-collisional tectonic setting.

As mentioned, the most striking features of the Shuangjianzishan granite porphyry are its low initial ⁸⁷Sr/⁸⁶Sr ratios, positive ε_{Nd}(*t*) values, Nd *T*_{DM2} ages (850–864 Ma) and high zircons ε_{Hf}(*t*) values (Tables 5 and 6), suggesting a high proportion of juvenile material in its petrogenesis. In order to provide a more generalized picture for the southern GXR, we further plotted additional published data describing the adjacent Haobugao deposit granite and regional Mesozoic granites for their Sr–Nd–Hf isotopic compositions. As shown in Figure 9a, all ε_{Hf}(*t*) spot results from the Shuangjianzishan granite porphyry, consistent with those of Haobugao, deviate from the ancient crustal evolution lines, suggesting that the Shuangjianzishan granite porphyry was derived from the

Table 5. Sr–Nd isotopic compositions of the Shuangjiazishan granite porphyry

Sample	Rb (ppm)	Sr (ppm)	$^{87}\text{Rb}/^{86}\text{Sr}$	$^{87}\text{Sr}/^{86}\text{Sr}$	2σ	$(^{87}\text{Sr}/^{86}\text{Sr})_t$	Sm (ppm)	Nd (ppm)	$^{147}\text{Sm}/^{144}\text{Nd}$	$^{143}\text{Nd}/^{144}\text{Nd}$	2σ	$(^{143}\text{Nd}/^{144}\text{Nd})_t$	$\epsilon_{\text{Nd}}(t)$	T_{DM2}
50-1	220	275	2.319	0.709774	16	0.70549	5.54	25	0.134	0.512621	10	0.512621	0.71	864
50-2	208	273	2.209	0.709663	16	0.70558	5.55	25.9	0.13	0.512626	10	0.512626	0.88	850
50-3	214	271	2.289	0.709795	22	0.70557	5.27	25.2	0.126	0.512619	12	0.512619	0.8	857

*Note: initial Sr and Nd isotopic ratios are calculated based on $t = 131$ Ma.

Table 6. Pb isotopic compositions of the Shuangjiazishan granite porphyry

Sample	U (ppm)	Th (ppm)	Pb (ppm)	$^{206}\text{Pb}/^{204}\text{Pb}$	2σ	$^{208}\text{Pb}/^{204}\text{Pb}$	2σ	$^{207}\text{Pb}/^{204}\text{Pb}$	2σ	$(^{206}\text{Pb}/^{204}\text{Pb})_t$	$(^{207}\text{Pb}/^{204}\text{Pb})_t$	$(^{208}\text{Pb}/^{204}\text{Pb})_t$
50-1	7.34	20.4	16	18.7196	10	38.532	12	15.5559	8	18.124	15.527	37.99
50-2	8.15	21.9	17	18.7413	14	38.5787	16	15.5584	12	18.118	15.528	38.03
50-3	8.2	22	26	18.6594	10	38.4653	12	15.5519	8	18.25	15.532	38.106

*Note: $(^{206}\text{Pb}/^{204}\text{Pb})_t$, $(^{207}\text{Pb}/^{204}\text{Pb})_t$ and $(^{208}\text{Pb}/^{204}\text{Pb})_t$ are Pb isotopic ratios at $t = 131$ Ma for the whole-rock of the Shuangjiazishan granite samples, calculated from the measured whole-rock U, Th and Pb contents and whole-rock Pb isotopic ratios.

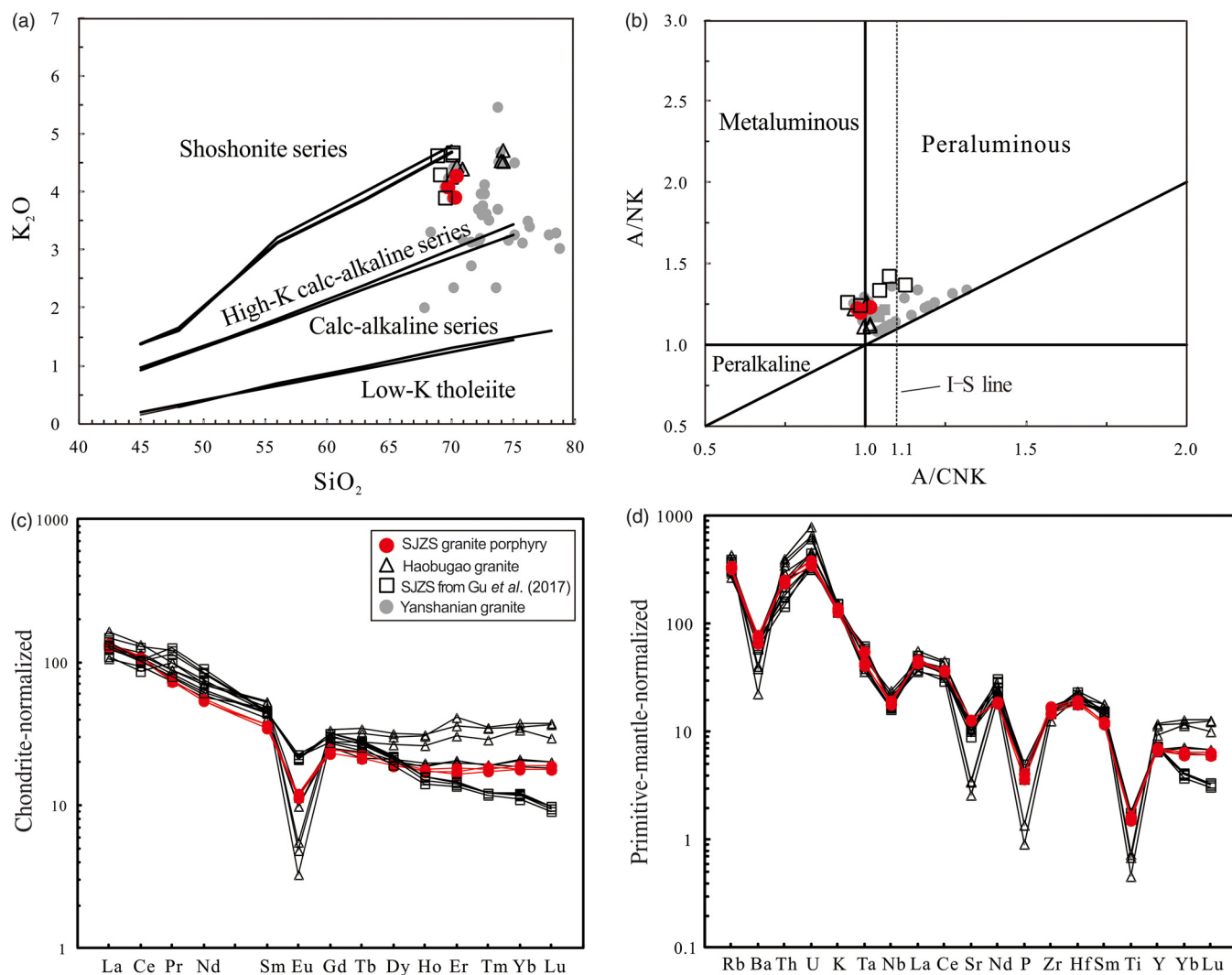


Fig. 7. (Colour online) (a) SiO_2 – K_2O discriminant plot (after Peccerillo & Taylor, 1976) for the Shuangjiazishan (SJZS) granite porphyry; (b) A/CNK – A/NK diagram (after Maniar & Piccoli, 1989) for the discriminant of metaluminous, peraluminous and peralkaline rocks; (c) chondrite-normalized REE pattern; and (d) primitive-mantle-normalized trace-element patterns. Primitive mantle and chondrite data are from Sun & McDonough (1989). Haobugao data are from Wang *et al.* (2018), the data represented by the square are from the SJZS granite (Gu *et al.* 2017) and Yanshanian granites data describing the southern GXR are from Mei *et al.* (2014), Ruan *et al.* (2015), Wang *et al.* (2016a) and Liu *et al.* (2017).

Table 7. Zircon Lu–Hf isotopic data of the Shuangjianzishan granite porphyry

Sample	$^{176}\text{Hf}/^{177}\text{Hf}$	1σ	$^{176}\text{Lu}/^{177}\text{Hf}$	1σ	$^{176}\text{Yb}/^{177}\text{Hf}$	1σ	$\epsilon_{\text{Hf}}(0)$	1σ	$\epsilon_{\text{Hf}}(t)$	1σ	T_{DM1} (Ma)	T_{DM2} (Ma)	$f_{\text{Lu/Hf}}$
1	0.282854	0.00002	0.000975	0.00001	0.031904	0.000307	2.9	0.9	5.7	0.9	564.4	736	−0.97
2	0.282866	0.000018	0.001293	0.000025	0.042981	0.001027	3.3	0.8	6.1	0.8	551	712	−0.96
3	0.282888	0.000021	0.000969	0.000039	0.02925	0.001483	4.1	0.9	6.9	0.9	515.7	668	−0.97
4	0.282873	0.00002	0.000959	0.00002	0.033785	0.000785	3.6	0.9	6.4	0.9	536.7	698	−0.97
5	0.282875	0.000018	0.001234	0.000011	0.040007	0.000331	3.6	0.8	6.4	0.8	538.2	696	−0.96
6	0.282833	0.000018	0.000989	0.00003	0.032094	0.000977	2.1	0.8	4.9	0.8	594.4	778	−0.97
7	0.282859	0.000018	0.001013	0.000016	0.032956	0.000705	3.1	0.8	5.9	0.8	556.7	725	−0.97
8	0.282865	0.000021	0.001345	0.000026	0.044177	0.000727	3.3	0.9	6.1	0.9	553.2	714	−0.96
9	0.282852	0.000016	0.000672	0.000005	0.02225	0.000135	2.8	0.8	5.6	0.8	562.7	738	−0.98
10	0.282854	0.000016	0.000884	0.000004	0.028714	0.000316	2.9	0.8	5.7	0.8	562.9	735	−0.97
11	0.282851	0.000015	0.000831	0.000007	0.026662	0.00039	2.8	0.7	5.6	0.7	565.6	740	−0.97
12	0.282853	0.000018	0.001363	0.000074	0.04343	0.002247	2.9	0.8	5.6	0.8	570.5	738	−0.96
13	0.28286	0.000017	0.000837	0.000008	0.028088	0.000537	3.1	0.8	5.9	0.8	553.2	722	−0.97
14	0.28285	0.000018	0.001111	0.000009	0.035443	0.000391	2.8	0.8	5.5	0.8	571.8	744	−0.97
15	0.282862	0.000017	0.00067	0.000004	0.026462	0.000587	3.2	0.8	6	0.8	548.4	718	−0.98

*Note: All spots are calculated based on $t = 131$ Ma for the Shuangjianzishan granite porphyry.

melting of mantle-derived juvenile component. The potential for an enriched mantle source could not be ruled out, as Wang *et al.* (2006b) proposed that Mesozoic volcanic rocks in the Songliao Basin could be derived from an enriched mantle source. The zircons of the Shuangjianzishan granite porphyry have similar Hf isotopic features as the Phanerozoic igneous rocks in the eastern CAOB (Fig. 9a; Wu & Sun, 1999; Yang *et al.* 2006; Sui *et al.* 2007), distinct from those in the NCC (Fig. 9a; Yang *et al.* 2006). Based on the mixing model proposed by Wu *et al.* (2000, 2002), it is obvious that most samples from the Shuangjianzishan granite porphyry plot close to the mixing lines of the mantle-derived juvenile components (*c.* 80%) and the lower crust (*c.* 20%), similar to those of regional Mesozoic A-type granites (Wu *et al.* 2003); this finding is also supported by the Pb isotopic compositions (Fig. 9c, d). The calculation by no means indicates that the granites were formed by mixing depleted mantle (DM) and lower continental crust (LCC) melts in such proportions. Rather, it suggests that the granitic magmas were produced by melting of a mixed lithology containing lower crustal components intruded or underplated by mantle-derived magma in such a proportion (Wu *et al.* 2003). Furthermore, mafic microgranular enclaves, which are significant evidence of magma mixing (Barbarin, 2005), have not been observed in this granite porphyry. Typical mineralogical textures representing magma mixing, such as quartz ocelli rimmed by hornblende and/or biotite and acicular apatite (Baxter & Feely, 2002), have not been found either (Fig. 4a). Accordingly, the small amount of crustal components involved in the magma formation may be due to assimilation occurring in the magma chamber or during magma uprising. Some studies suggested that the generation of such voluminous granites should be related to the melting of heated crust induced from upwelling of the asthenosphere in the late stage of orogenesis or subduction (Wu *et al.* 2000). We propose that, following oceanic closure, asthenospheric mantle melting during the Neoproterozoic Era led to mafic underplating in the lower crust, with which it interacted; these were subsequently melted to produce the Shuangjianzishan granite porphyry.

6.c. Tectonic implications

The peak of the outbreak of volcanic rocks and A-type granites in NE China occurred during the Cretaceous Period, which was also an important period for asthenospheric upwelling, lithospheric thinning and crustal stretching (Wu *et al.* 2002), as well as the peak of large-scale magma-thermal events in the Xingmeng Orogenic Belt (Wu *et al.* 2005a; Wang *et al.* 2006a; Zhang *et al.* 2010). In the southern GXR, a special geological structure was developed where the Palaeo-Asian and the Palaeo-Pacific tectonic domains overlap. The tectonic setting for the Shuangjianzishan deposit, the Haobugao deposit, and other deposits could be revealed by the presence of A-type granites associated with mineralization, which can form in both post-orogenic and anorogenic settings (Sylvester, 1989; Bonin, 1990; Eby, 1992; Nedelec *et al.* 1995). Eby (1992) sub-divided A-type granites into A₁ and A₂ groups; the A₁ group represents an anorogenic setting and the A₂ group represents a variety of tectonic environments. The Shuangjianzishan granite samples, consistent with the Haobugao granite, mainly fall within the A₂ group (Figs 8d, 10a, b), suggesting that they formed in a post-orogenic extensional environment.

As mentioned in Section 6.b, the Shuangjianzishan granite porphyry was the result of extensive partial melting of mantle-derived juvenile crust, synchronous with the Early Cretaceous magmatism spanning the entire GXR, which is envisaged to have formed in a lithospheric extensional environment (Li *et al.* 2008). In addition, widespread volcanic rocks (137 Ma) exposed around Shuangjianzishan are basically coeval with the Early Cretaceous granite porphyry (Wang *et al.* 2018). It was recognized by previous researchers that the intrusive rocks formed in an extensional environment (Wang *et al.* 2018). Furthermore, the generation of A-type granites requires a high melting temperature (Clemens *et al.* 1986), and the upwelling of the asthenosphere could provide the heat necessary to produce a considerable volume of A-type granites in NE China during late Mesozoic time in this extensional setting (Wu *et al.* 2002).

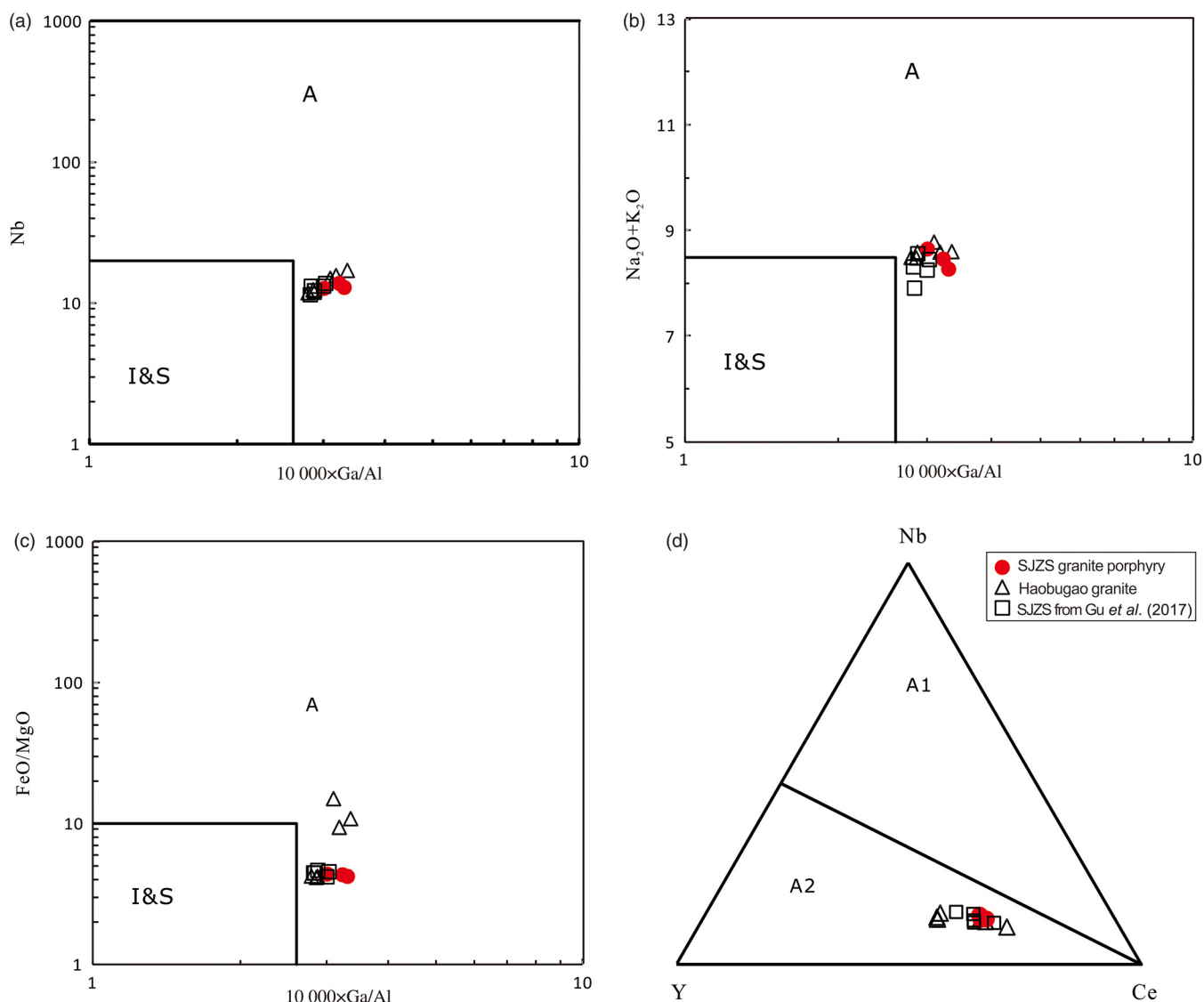


Fig. 8. (Colour online) Discrimination diagrams of (a) Nb versus $10\,000 \times \text{Ga}/\text{Al}$; (b) $\text{Na}_2\text{O} + \text{K}_2\text{O}$ versus $10\,000 \times \text{Ga}/\text{Al}$; (c) FeO/MgO versus $10\,000 \times \text{Ga}/\text{Al}$; (d) Nb-Y-Ce (after Whalen *et al.* 1987; Eby, 1992). Triangle points are from Wang *et al.* (2018) and the square from Gu *et al.* (2017). A₁ – anorogenic setting; A₂ – post-collisional setting.

To date, two possible models have been proposed for this extensional setting: (1) delamination of the lower crust induced by the subduction of the Palaeo-Pacific Plate (Wu *et al.* 2005b; Wang *et al.* 2006a; Zhang *et al.* 2008, 2010); and (2) post-orogenic lithospheric extension related to the closure of the Mongol–Okhotsk Ocean (Fan *et al.* 2003; Meng, 2003). As previous studies have suggested, the Mongol–Okhotsk Ocean closed during the Middle and Late Jurassic epochs (Zorin, 1999), and the Pacific Plate has expanded considerably since the Late Cretaceous Epoch (Larson *et al.* 1985), so the Shuangjianzishan granite porphyry U–Pb age of 131 Ma coincides with post-orogenic extension following the closure of the Mongol–Okhotsk Ocean. Furthermore, Mesozoic volcanic magmatism in the southern GXR shows a NE-trending linear distribution that gradually ages from west to east (125–160 Ma) (Wang *et al.* 2006b), consistent with the Mongol–Okhotsk Ocean closing direction from west to east (Metelkin *et al.* 2010). Gu *et al.* (2017) believe the regional tectonic stress in the southern GXR is tensional and that the Mongol–Okhotsk Ocean closing direction favours the reduction in pressure within the plate.

However, the subduction of the Palaeo-Pacific Ocean Plate caused large-scale back-arc extension of NE China and is not dominant in this region (Dong *et al.* 2014; Ma *et al.* 2015). Accordingly, it can be conjectured that the Early Cretaceous extensional setting in the southern GXR mainly resulted from the upwelling of asthenospheric mantle in the post-orogenic period of Mongol–Okhotsk Ocean closure.

7. Conclusions

1. Zircon LA-ICP-MS U–Pb dating confirms that the Shuangjianzishan granite porphyry in the southern GXR formed during the Early Cretaceous Epoch (131 ± 1 Ma).
2. The petrography, geochemistry and isotope compositions indicate that the Shuangjianzishan granite porphyry belongs to metaluminous to peraluminous high-K calc-alkaline A-type granite, and is derived from the partial melting of mantle-derived juvenile component (*c.* 80%), contaminated by assimilation of a low proportion of the lower crust (*c.* 20%).

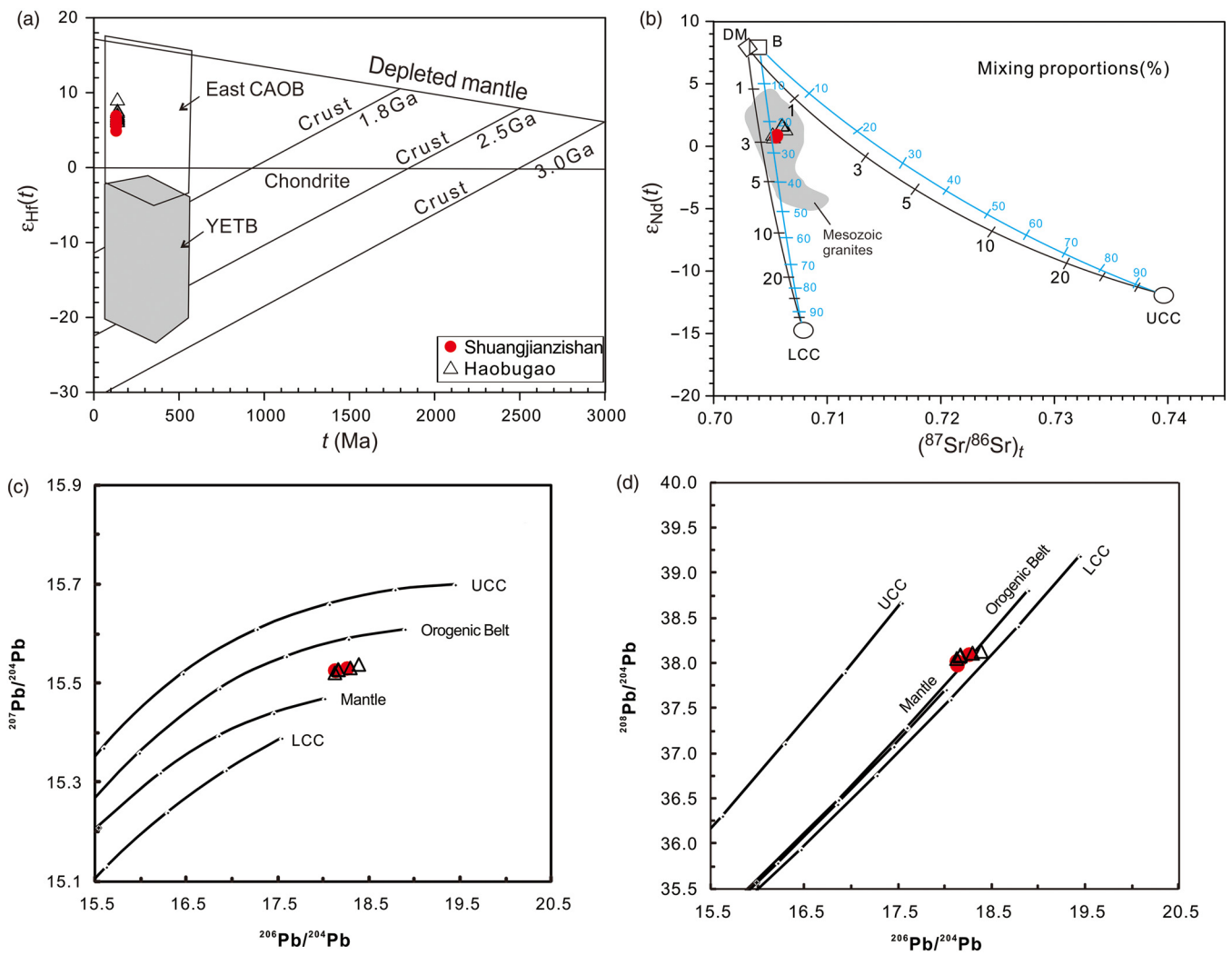


Fig. 9. (Colour online) (a) Mantle: plot of $\epsilon_{\text{Hf}}(t)$ versus t (Ma) for the zircons from the Shuangjiazishan granite porphyry. CAOB – the Central Asian Orogenic Belt; YFTB – Yanshan Fold and Thrust Belt (Yang *et al.* 2006). (b) Orogene: $\epsilon_{\text{Nd}}(t)$ versus $(^{87}\text{Sr}/^{86}\text{Sr})_t$ isotopic ratio plot showing mixing proportions between two end-members (after Wu *et al.* 2003): (1) depleted mantle or juvenile components (DM – upper mantle peridotite; B – basalt) and (2) crustal components (LCC – lower continental crust; UCC – upper continental crust; both represented by the Mashan gneisses in the Jiamusi Block; Wu *et al.* 2000). The grey area represents Mesozoic granites from Wu *et al.* (2003). (c) Upper crust: $^{207}\text{Pb}/^{204}\text{Pb}$ versus $^{206}\text{Pb}/^{204}\text{Pb}$ diagram and (d) lower crust: $^{208}\text{Pb}/^{204}\text{Pb}$ versus $^{206}\text{Pb}/^{204}\text{Pb}$ diagram for distinguishing tectonic setting (after Zartman & Doe, 1981). Haobugao data Wang *et al.* (2018).

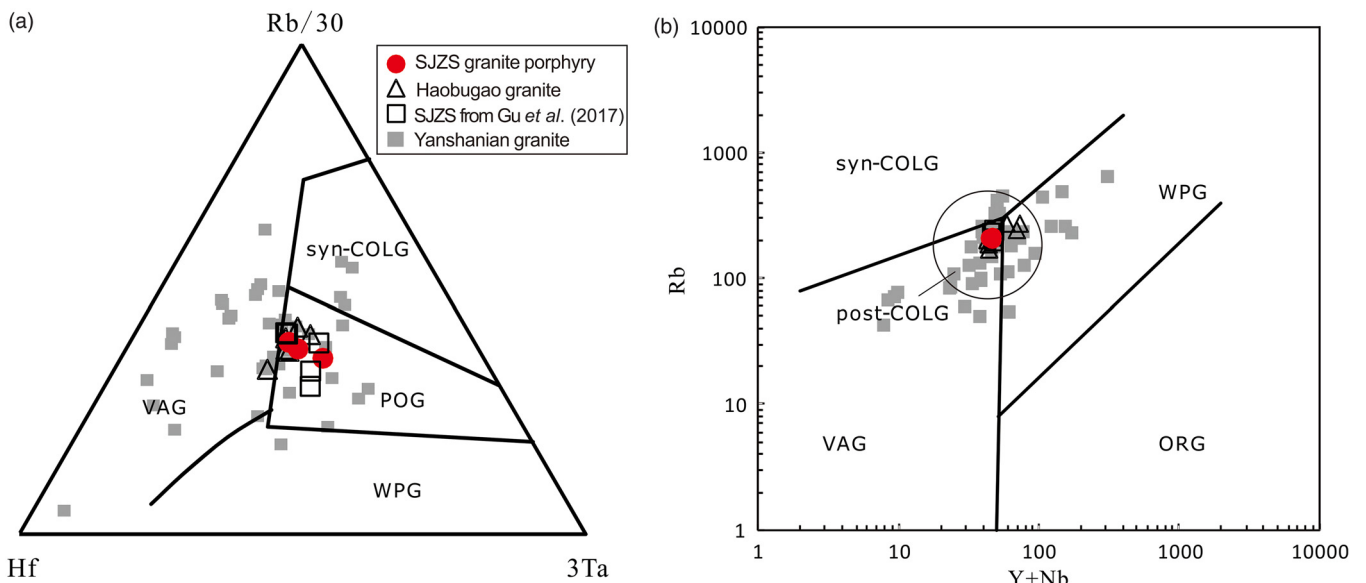


Fig. 10. (Colour online) (a) (Rb/30)-Hf-3Ta discrimination diagram (after Harris *et al.* 1986); (b) Rb versus (Yb+Ta) discrimination diagram (after Pearce, 1996). VAG – volcanic-arc granite; ORG – ocean-ridge granite; WPG – within-plate granite; COLG – collision granite; POG – post-collision granite. Triangle points are from Wang *et al.* (2018) and the grey-shaded squares from Mei *et al.* (2014), Ruan *et al.* (2015), Wang *et al.* (2016a) and Liu *et al.* (2017).

3. The Shuangjianzishan granite porphyry was emplaced in a post-orogenic extensional environment related to the asthenosphere upwelling followed the Mongol–Okhotsk Ocean closure.

Acknowledgements. We thank colleagues for their assistance and Tiantong Geological Exploration Co. Ltd., Chifeng, Inner Mongolia, China for support during fieldwork. This research was supported by the Inner Mongolia Autonomous Region Geological Prospecting Fund Management Center (grant no. NMKD2014-23), China Geological Survey (grant no. 121201009000150011) and China Postdoctoral Science Foundation (grant no. 2015M582300). The anonymous reviewers are gratefully acknowledged for their constructive and valuable comments.

References

- Amelin Y, Lee DC and Halliday AN** (2000) Early-Middle Archean crustal evolution deduced from Lu–Hf and U–Pb isotopic studies of single zircon grains. *Geochimica et Cosmochimica Acta* **64**, 4205–25.
- Barbarin B** (2005) Mafic magmatic enclaves and mafic rocks associated with some granitoids of the central Sierra Nevada batholith, California: nature, origin, and relations with the hosts. *Lithos* **80**, 155–77.
- Baxter S and Feely M** (2002) Magma mixing and mingling textures in granitoids: examples from the Galway Granite, Connemara, Ireland. *Mineralogy and Petrology* **76**, 63–74.
- Bonin B** (1990) From orogenic to anorogenic settings: evolution of granitoid suites after a major orogenesis. *Geological Journal* **25**, 261–70.
- Chappell BW** (1984) Source rocks of I- and S-type granites in the Lachlan Fold Belt, southeastern Australia. *Philosophical Transactions of the Royal Society of London A* **310**, 693–707.
- Chappell BW** (1999) Aluminium saturation in I- and S-type granites and the characterization of fractionated hapogranites. *Lithos* **46**, 535–51.
- Chappell BW, Bryant CJ and Wyborn D** (2012) Peraluminous I-type granites. *Lithos* **153**, 142–53.
- Chappell BW and White AJR** (1974) Two contrasting granite types. *Pacific Geology* **8**, 173–74.
- Chappell BW and White AJR** (1992) I- and S-type granites in the Lachlan Fold Belt. *Transactions of the Royal Society of Edinburgh: Earth Sciences* **83**, 1–26.
- Chen H, Xia QK, Ingrin J, Deloué E and Bi Y** (2017) Heterogeneous source components of intraplate basalts from NE China induced by the ongoing Pacific slab subduction. *Earth & Planetary Science Letters* **459**, 208–20.
- Clemens JD, Holloway JR and White AJR** (1986) Origin of an A-type granite: experimental constraints. *American Mineralogist* **71**, 317–24.
- Cogné JP, Kravchinsky VA, Halim N and Hankard F** (2005) Late Jurassic–Early Cretaceous closure of the Mongol–Okhotsk Ocean demonstrated by new Mesozoic palaeomagnetic results from the Trans-Baikal area (SE Siberia). *Geophysical Journal International* **63**, 813–32.
- Collins WJ, Beams SD, White AJR and Chappell BW** (1982) Nature and origin A-type granites with particular reference to Southeastern Australia. *Contributions to Mineralogy and Petrology* **80**, 189–200.
- Cui M** (2015) *The geochemical characteristics and diagenesis of ore-forming diorite-porphyrite from Shuangjianzishan Ag polymetallic deposit in Inner Mongolia*. M.Sc. thesis, Mineral Deposit and Mineral Deposit Geochemistry, China University of Geosciences (Beijing). Published thesis.
- Dong Y, Ge WC, Yang H, Zhao GH, Wang QH, Zhang YL and Su L** (2014) Geochronology and geochemistry of Early Cretaceous volcanic rocks from the Baiyingaolao Formation in the central Great Xing’an Range, NE China, and its tectonic implications. *Lithos* **205**, 168–84.
- Eby GN** (1992) Chemical subdivision of the A-type granitoids: petrogenetic and tectonic implications. *Geology* **20**, 641–44.
- Fan WM, Guo F, Wang YJ and Lin G** (2003) Late Mesozoic calc-alkaline volcanism of post-orogenic extension in the northern DaHinggan Mountains, Northeastern China. *Journal of Volcanology and Geothermal Research* **121**, 115–35.
- Fritzell EH, Bull AL and Shephard GE** (2016) Closure of the Mongol–Okhotsk Ocean: insights from seismic tomography and numerical modelling. *Earth & Planetary Science Letters* **445**, 1–12.
- Gu YC, Chen RY, Jia B and Ju N** (2017) Zircon U–Pb dating and geochemistry of the granite porphyry from the Shuangjianzishan silver polymetallic deposit in Inner Mongolia and tectonic implication. *Geology and Exploration* **53**, 495–507 (in Chinese).
- Harris NBW, Pearce JA and Tindle AG** (1986) Geochemical characteristics of collision-zone magmatism. In *Collision Tectonics* (eds MP Coward and AC Reis), pp. 67–81. Geological Society of London, Special Publication no. 19.
- Hineab R, Williams IS, Chappelle BW and White AJR** (1978) Contrasts between I- and S-type granitoids of the Kosciusko Batholith. *Journal of the Geological Society of Australia* **25**, 219–34.
- Hu Z, Liu Y, Gao S, Liu WG, Zhang W, Tong XR, Lin L, Zong KQ, Li M, Chen HH, Zhou L and Yang L** (2012) Improved in situ Hf isotope ratio analysis of zircon using newly designed X skimmer cone and jet sample cone in combination with the addition of nitrogen by laser ablation multiple collector ICP-MS. *Journal of Analytical Atomic Spectrometry* **27**, 1391–99.
- Jahn BM, Wu FY, Capdeviala R, Fourcade S, Wang YX and Zhao ZH** (2001) Highly evolved juvenile granites with tetrad REE patterns: the Woduhe and Baerzhe granites from the Great Xing’an (Khingan) Mountains in NE China. *Lithos* **59**, 171–98.
- Jiang BB, Zhu XY, Huang XK, Xu Q and Zhang ZQ** (2017) Isotopic characteristics of sulfur and lead and metallogenic mechanism of Shuangjianzishan silver polymetallic deposit in Inner Mongolia. *Mineral Exploration* **8**, 1010–19 (in Chinese).
- Jiang SH, Nie FJ, Bai DM, Liu YF and Liu Y** (2011) Geochronology evidence for Indosinian mineralization in Baiyinnuoer Pb–Zn deposit of Inner Mongolia. *Mineral Deposits* **30**, 787–98 (in Chinese with English abstract).
- Kelty TK, Yin A, Dash B, Gehrels GE and Ribeiro AE** (2008) Detrital-zircon geochronology of Paleozoic sedimentary rocks in the Hangay–Hentey basin, north-central Mongolia: implications for the tectonic evolution of the Mongol–Okhotsk Ocean in central Asia. *Tectonophysics* **451**, 290–311.
- Koschek G** (1993) Origin and significance of the SEM cathodoluminescence from zircon. *Journal of Microscopy* **171**, 223–32.
- Kravchinsky VA, Cogné JP, Harbert WP and Kuzmin MI** (2002) Evolution of the Mongol–Okhotsk Ocean as constrained by new palaeomagnetic data from the Mongol–Okhotsk suture zone, Siberia. *Geophysical Journal International* **148**, 34–57.
- Kuang YS, Zheng GR, Lu MJ, Liu YL, Zhang SJ, Li Y and Cheng WJ** (2014) Basic characteristics of Shuangjianzishan silver polymetallic deposit in Chifeng City, Inner Mongolia. *Mineral Deposits* **33**, 847–56 (in Chinese).
- Larson RL, Pitman WC, Golovchenko X, Cande SC, Dewey JF, Haxby WF and La Brecque JL** (1985) *The Bedrock Geology of the World*. New York: WH Freeman and Company.
- Li JW, Zhao XF, Zhou MF, Vasconcelos P, Ma CQ, Deng XD, Souza ZS, Zhao YX and Wu G** (2008) Origin of the Tongshankou porphyry–skarn Cu–Mo deposit, eastern Yangtze craton, Eastern China: geochronological, geochemical, and Sr–Nd–Hf isotopic constraints. *Mineralium Deposita* **43**, 315–36.
- Li JY, Guo F, Li CW, Li HX and Zhao L** (2014) Neodymium isotopic variations of Late Paleozoic to Mesozoic I- and A-type granitoids in NE China: implications for tectonic evolution. *Acta Petrologica Sinica* **30**, 1995–2008 (in Chinese with English abstract).
- Li PZ and Yu JS** (1993) Nianzishan miarolitic alkaline granite stock, Heilongjiang – its ages and geological implications. *Geochimica* **22**, 389–97 (in Chinese with English abstract).
- Li XH, Liu DY, Sun M, Li WX, Liang XR and Liu Y** (2004) Precise Sm–Nd and U–Pb isotopic dating of the super-giant Shizhuyuan polymetallic deposit and its host granite, Southeast China. *Geological Magazine* **141**, 225–231.
- Li XH and McCulloch MT** (1998) Geochemical characteristics of Cretaceous mafic dikes from Northern Guangdong, SE China: age, origin and tectonic significance. In *Mantle Dynamics and Plate Interactions in East Asia* (eds MFJ Flower, SL Chung, CH Lo and YT Lee), pp. 405–19. Washington: American Geophysical Union **27**, 405–19.
- Liu CH, Bagas L and Wang F** (2016) Isotopic analysis of the super-large Shuangjianzishan Pb–Zn–Ag deposit in Inner Mongolia, China: constraints on magmatism, metallogenesis, and tectonic setting. *Ore Geology Reviews* **75**, 252–267.
- Liu HZ** (2017) *Discussion on Metallogenic characteristics and Genesis of Weilasituo Sn Polymetal Deposit in Inner Mongolia*. Ph.D. thesis, China University of Geosciences (Beijing). Published thesis.

- Liu K, Zhang JJ, Wilde SA, Zhou JB, Wang M, Ge MH, Wang JM and Ling YY (2017) Initial subduction of the Paleo-Pacific oceanic plate in NE China: constraints from whole-rock geochemistry and zircon U-Pb and Lu-Hf isotopes of the Khanka Lake granitoids. *Lithos* **274**, 254–70.
- Liu YS, Gao S, Hu ZC, Gao CG, Zong KQ and Wang DB (2010) Continental and oceanic crust recycling-induced melt-peridotite interactions in the Trans-North China Orogen: U-Pb dating, Hf isotopes and trace elements in zircons of mantle xenoliths. *Journal of Petrology* **51**, 537–71.
- Liu YS, Hu ZC, Gao S, Gunther D, Xu J, Gao CG and Chen HH (2008) In situ analysis of major and trace elements of anhydrous minerals by LA-ICP-MS without applying an internal standard. *Chemical Geology* **257**, 34–43.
- Liu Y, Jiang SH, Leon B, Chen CL, Han N and Wan YY (2020) Petrogenesis and metallogenetic potential of the Wulanba granite, southern Great Xing'an Range, NE China: constraints from whole-rock and apatite geochemistry. *Geological Magazine* **157**(3), 411–34.
- Ludwig KR (2003) *User's Manual for Isoplot 3.0-a Geochronological Toolkit for Microsoft Excel*. Berkeley Geochronology Center, Special Publication **4**, 1–70.
- Ma XH, Cao R, Zhou ZH and Zhu WP (2015) Early Cretaceous high-Mg diorites in the Yanji area, northeastern China: petrogenesis and tectonic implications. *Journal of Asian Earth Sciences* **97**, 393–405.
- Maniar PD and Piccoli PM (1989) Tectonic discrimination of granitoids. *Geological Society of America Bulletin* **101**, 635–43.
- Mei W, Lv XB, Cao XF, Liu Z, Zhao Y, Ai ZL, Tang RK and Munir MA (2014) Ore genesis and hydrothermal evolution of the Huanggang skarn iron-tin polymetallic deposit, southern Great Xing'an Range: evidence from fluid inclusions and isotope analyses. *Ore Geology Reviews* **64**, 239–52.
- Mei W, Lv XB, Liu Z, Tang RK, Ai ZL, Wang XD and Cisse M (2015) Geochronological and geochemical constraints on the ore-related granites in Huanggang deposit, Southern Great Xing'an Range, NE China and its tectonic significance. *Geosciences Journal* **19**, 53–67.
- Meng QR (2003) What drove late Mesozoic extension of the northern China-Mongolia tract? *Tectonophysics* **369**, 155–74.
- Metelkin DV, Vemikovsky VA and Kazansky AY (2010) Late Mesozoic tectonics of central Asia based on paleomagnetic evidence. *Gondwana Research* **18**, 400–19.
- Miao LC, Liu DY, Zhang FQ, Fan WM, Shi YR and Xie HQ (2007) Zircon SHRIMP U–Pb ages of the “Xinghuadukou Group” in Hanjiayuanzi and Xinlin areas and the “Zhalantun Group” in Inner Mongolia, Da Hinggan Mountains. *Chinese Science Bulletin* **52**, 1112–24.
- Nedelec A, Stephens WE and Fallick AE (1995) The Panafrican stratoid granites of Madagascar: alkaline magmatism in a post-collisional extensional setting. *Journal of Petrology* **36**, 1367–91.
- Ouyang HG, Li RH and Zhou ZH (2016) The Jurassic mineralization of the Shuangjianzishan Ag-polymetallic deposit and its significance in prospecting: evidence from geochronology. *Acta Geologica Sinica* **90**, 1835–45 (in Chinese).
- Ouyang HG, Mao JW and Santosh M (2013) Anatomy of a large Ag-Pb-Zn deposit in the Great Xing'an Range, northeast China: metallogeny associated with Early Cretaceous magmatism. *International Geology Review* **55**, 411–29.
- Ouyang HG, Mao JW, Santosh M, Wu Y, Hou L and Wang XF (2014) The Early Cretaceous Weilasituo Zn-Cu-Ag vein deposit in the southern Great Xing'an Range, northeast China: fluid inclusions, H, O, S, Pb isotope geochemistry and genetic implications. *Ore Geology Review* **56**, 503–15.
- Ouyang HG, Mao JW, Zhou ZH and Su HM (2015) Late Mesozoic metallogeny and intracontinental magmatism, southern Great Xing'an Range, northeastern China. *Gondwana Research* **27**, 1153–72.
- Pan XF, Guo LJ, Wang S, Xue HM, Hou ZQ, Tong Y and Li ZM (2009) Laser microprobe Ar-Ar dating of biotite from the Weilasituo Cu-Zn polymetallic deposit in Inner Mongolia. *Acta Petrologica et Mineralogica* **28**, 475–79 (in Chinese with English abstract).
- Pearce JA (1996) Sources and settings of granitic rocks. *Episodes* **19**, 120–25.
- Peccerillo A and Taylor SR (1976) Geochemistry of Eocene calc-alkaline volcanic rocks from the Kastamonu area, northern Turkey. *Contributions to Mineralogy and Petrology* **58**, 63–81.
- Pei F, Xu W, Yang D, Zhao Q, Liu X and Hu Z (2007) Zircon U–Pb geochronology of basement metamorphic rocks in the Songliao Basin. *Chinese Science Bulletin* **52**, 942–48.
- Pupin JP (1980) Zircon and granite petrology. *Contributions to Mineralogy and Petrology* **73**, 207–20.
- Ruan BX, Lv XB, Yang W, Liu ST, Yu YM, Wu CM and Munir MAA (2015) Geology, geochemistry and fluid inclusions of the Bianjiadayuan Pb-Zn-Ag deposit, Inner Mongolia, NE China: implications for tectonic setting and metallogeny. *Ore Geology Reviews* **71**, 121–37.
- Shu QH, Lai Y, Sun Y, Wang C and Meng S (2013) Ore genesis and hydrothermal evolution of the Baiyinnuo'er zinc-lead skarn deposit, Northeast China: evidence from isotopes (S, Pb) and fluid inclusions. *Economic Geology* **108**, 835–60.
- Sui ZM, Ge WC, Wu FY, Zhang JH, Xu XC and Chang RY (2007) Zircon U-Pb ages, geochemistry and its petrogenesis of Jurassic granites in northeastern part of the Da Hinggan Mts. *Acta Petrologica Sinica* **23**, 461–80 (in Chinese with English abstract).
- Sun DY, Wu FY, Li HM and Lin Q (2000) Emplacement age of the postorogenic A-type granites in northwestern Lesser Xing'an Ranges, and its relationship to the eastward extension of Suolunshan-Hegenshan-Zhalaithe collisional suture zone. *Chinese Science Bulletin* **45**, 2217–22 (in Chinese with English abstract).
- Sun SS and McDonough WF (1989) Chemical and isotopic systematics of oceanic basalt: implication for mantle composition and processes. In *Magmatism in the Ocean Basin* (eds AD Saunders and MJ Morry), pp. 528–48. Geological Society of London, Special Publication no. 42.
- Sylvester PJ (1989) Post-collisional alkaline granites. *Journal of Geology* **97**, 261–80.
- Tang J, Xu WL, Wang F, Zhao S and Wang W (2016) Early Mesozoic southward subduction history of the Mongol-Okhotsk oceanic plate: evidence from geochronology and geochemistry of Early Mesozoic intrusive rocks in the Erguna Massif, NE China. *Gondwana Research* **31**, 218–40.
- Tang ZY, Sun DY and Mao AQ (2020) Geochemistry of Late Mesozoic volcanic rocks in the central Great Xing'an Range, NE China: petrogenesis and crustal growth in comparison with adjacent areas. *International Geology Review* **62**(1), doi: [10.1080/00206814.2019.1590867](https://doi.org/10.1080/00206814.2019.1590867).
- Tian DX, Ge WC, Yang H, Zhao GC and Zhang YL (2014) Lower Cretaceous alkali feldspar granites in the central part of the Great Xing'an Range, northeastern China: chronology, geochemistry and tectonic implications. *Geological Magazine* **152**, 383–99.
- Wang FX, Sun HJ, Pei RF, Liu YF, Liu CH and Jiang SH (2016a) The geologic features and genesis of Shuangjianzishan Silver-Polymetallic deposit, Balinzuo Qi, Inner Mongolia. *Geological Review* **62**, 1242–56 (in Chinese).
- Wang F, Zhou XH, Zhang LC, Ying JF, Zhang YT, Wu FY and Zhu RX (2006a) Late Mesozoic volcanism in the Great Xing'an Range (NE China): timing and implications for the dynamic setting of NE Asia. *Earth and Planetary Science Letters* **251**, 179–98.
- Wang PJ, Chen FK, Chen SM, Wolfgang S and Muharrem S (2006b) Geochemical and Nd-Sr-Pb isotopic composition of Mesozoic volcanic rocks in the Songliao basin, NE China. *Geochemical Journal* **40**, 149–59.
- Wang XD, Xu DM, Lv XB, Wei W, Mei W, Fan XJ and Sun BK (2018) Origin of the Haobugao skarn Fe-Zn polymetallic deposit, Southern Great Xing'an range, NE China: geochronological, geochemical, and Sr-Nd-Pb isotopic constraints. *Ore Geology Reviews* **94**, 58–72.
- Wang ZJ, Xu WL, Pei FP, Wang ZW, Li Y and Cao HH (2015) Geochronology and geochemistry of middle Permian-Middle Triassic intrusive rocks from central-eastern Jilin Province, NE China: constraints on the tectonic evolution of the eastern segment of the Paleo-Asian Ocean. *Lithos* **238**, 13–25.
- Wang ZW, Pei FP, Xu WL, Cao HH, Wang ZJ and Zhang Y (2016b) Tectonic evolution of the eastern Central Asian Orogenic Belt: evidence from zircon U-Pb-Hf isotopes and geochemistry of early Paleozoic rocks in Yanbian region, NE China. *Gondwana Research* **38**, 334–50.
- Wei GJ, Liang XR, Li XH and Liu Y (2002) Precise measurement of Sr isotopic composition of liquid and solid base using (LP) MC-ICP-MS. *Geochimica* **31**, 295–99 (in Chinese with English abstract).
- Whalen JB, Currie KL and Chappell BW (1987) A-type granites: geochemical characteristics, discrimination and petrogenesis. *Contributions to Mineralogy and Petrology* **95**, 407–19.
- Wu FY, Jahn BM, Wilde SA, Lo CH, Yui TF, Lin Q, Ge WC and Sun DY (2003) Highly fractionated I-type granites in NE China (II): isotopic

- geochemistry and implications for crustal growth in the Phanerozoic. *Lithos* **67**, 191–204.
- Wu FY, Jahn BM, Wilde SA and Sun DY** (2000) Phanerozoic crustal growth: U-Pb and Sr-Nd isotopic evidence from the granites in northeastern China. *Tectonophysics* **328**, 89–113.
- Wu FY, Lin J, Wilde SA, Zhang XO and Yang JH** (2005a) Nature and significance of the Early Cretaceous giant igneous event in eastern China. *Earth and Planetary Science Letters* **233**, 103–19.
- Wu FY and Sun DY** (1999) The Mesozoic magmatism and lithospheric thinning in Eastern China. *Journal of Changchun Science and Technology University* **29**, 313–8 (in Chinese with English abstract).
- Wu FY, Sun DY, Ge WC, Zhang YB, Grant ML, Wilde SA and Jahn BM** (2011) Geochronology of the Phanerozoic granitoids in northeastern China. *Journal of Asian Earth Sciences* **41**, 1–30.
- Wu FY, Sun DY, Li HM, Jahn BM and Wilde S** (2002) A-type granites in northeastern China: age and geochemical constraints on their petrogenesis. *Chemical Geology* **187**, 143–73.
- Wu FY, Yang JH, Lo CH, Wilde SA, Sun DY and Jahn BM** (2007) The Heilongjiang Group a Jurassic accretionary complex in the Jiamusi Massif at the western Pacific margin of northeastern China. *Island Arc* **16**, 156–72.
- Wu FY, Yang JH, Wilde SA and Zhang XO** (2005b) Geochronology, petrogenesis and tectonic implications of the Jurassic granites in the Liaodong Peninsula, NE China. *Chemical Geology* **221**, 127–56.
- Wu GB, Liu JM, Zeng QD, Liu MT, Sun HS, Yin ZW and Yin X** (2014) Occurrences of silver in the Shuangjianzishan Pb-Zn-Ag deposit and its implications for mineral processing. *Earth Science Frontiers* **21**, 105–15.
- Wu GB, Liu JM, Zeng QD, Sun HS and Liu MT** (2013) Metallogenic age of the Shuangjianzishan Pb-Zn-Ag deposit in Great Xing'an Range, Inner Mongolia. *Acta Mineralogica Sinica* **33**, Supplement(619), 619 (in Chinese).
- Wu G, Sun FY, Zhao CS, Li ZT, Zhao AL, Pang QB and Li GY** (2005c) Discovery of the Early Paleozoic post-collisional granites in northern margin of the Erguna massif and its geological significance. *Chinese Science Bulletin* **50**, 2733–43.
- Xu JF and Castillo PR** (2004) Geochemical and Nd-Pb isotopic characteristics of the Tethyan asthenosphere: implications for the origin of the Indian Ocean mantle domain. *Tectonophysics* **393**, 9–27.
- Xu JF, Castillo PR, Li XH, Yu XY, Zhang BR and Han YW** (2002) MORB-type rocks from the Paleo-Tethyan Mian-Lueyang northern ophiolite in the Qinling Mountains, central China: implications for the source of the low $^{206}\text{Pb}/^{204}\text{Pb}$ and high $^{143}\text{Nd}/^{144}\text{Nd}$ mantle component in the Indian Ocean. *Earth & Planetary Science Letters* **198**, 323–37.
- Yang JH, Wu FY, Shao JA, Wilde SA, Xie LW and Liu XM** (2006) Constraints on the timing of uplift of the Yanshan Fold and Thrust Belt, North China. *Earth and Planetary Science Letters* **246**, 336–52.
- Yang WB, Niu HC, Shan Q, Sun WD, Zhang H, Li NB, Jiang YH and Yu XY** (2013) Geochemistry of magmatic and hydrothermal zircon from the highly evolved Baerzhe alkaline granite: implications for Zr-REE-Nb mineralization. *Mineralium Deposita* **49**, 451–70.
- Yang Y, Gao FH, Chen JS, Zhou Y, Zhang J, Jin X and Zhang YL** (2012) Zircon U-Pb ages of Mesozoic volcanic rocks in Chifeng area. *Journal of Jilin University* **42**, 257–68 (in Chinese with English abstract).
- Ying JF, Zhou XH, Zhang LC and Wang F** (2010) Geochronological framework of Mesozoic volcanic rocks in the Great Xing'an Range, NE China, and their geodynamic implications. *Journal of Asian Earth Sciences* **39**, 786–93.
- Zartman RE and Doe BR** (1981) Plumbotectonics – the model. *Tectonophysics* **75**, 135–62.
- Zeng QD, Qin KZ, Liu JM, Li GM, Zhai MG, Chu SX and Guo YP** (2015) Porphyry molybdenum deposits in the Tianshan-Xingmeng orogenic belt, northern China. *International Journal of Earth Sciences* **104**, 991–1023.
- Zhai DG, Anthony EW-J, Liu JJ, David S, Panagiotis CV, Stylianos T, Li K, Li PL and Sun HJ** (2020) The Genesis of the giant Shuangjianzishan epithermal Ag-Pb-Zn deposit, Inner Mongolia, Northeastern China. *Economic Geology* **115**, 101–28.
- Zhai DG, Liu JJ, Li JM, Zhang M, Li BY, Fu X, Jiang HC, Ma LJ and Qi L** (2016) Geochronological study of Weilasituo porphyry type Sn deposit in Inner Mongolia and its geological significance. *Mineral Deposits* **35**, 1011–22 (in Chinese).
- Zhai DG, Liu JJ, Zhang HY, Yao MJ, Wang JP and Yang YQ** (2014) S-Pb isotopic geochemistry, U-Pb and Re-Os geochronology of the Huanggangliang Fe-Sn deposit, Inner Mongolia, NE China. *Ore Geology Reviews* **59**, 109–122.
- Zhang HF, Parrish R, Zhang L, Xu WC, Yuan HL, Gao S and Crowley QG** (2007) A-type granite and adakitic magmatism association in Songpan-Garze fold belt, eastern Tibetan Plateau: implication for lithospheric delamination. *Lithos* **97**, 323–35.
- Zhang JH, Gao S, Ge WC, Wu FY, Yang JH, Wilde SA and Li M** (2010) Geochronology of the Mesozoic volcanic rocks in the Great Xing'an Range, northeastern China: implications for subduction-induced delamination. *Chemical Geology* **276**, 144–65.
- Zhang JH, Ge WC, Wu FY, Wilde SA, Yang JH and Liu XM** (2008) Large-scale Early Cretaceous volcanic events in the northern Great Xing'an Range, Northeastern China. *Lithos* **102**, 138–57 (in Chinese with English abstract).
- Zhang ZQ** (2018) *Geological and geochemical characteristics and metallogenetic mechanism of the Shuangjianzishan Ag-polymetallic deposit, Inner Mongolia*. M.Sc. thesis, Geology and Geochemistry of Ore Deposit, China University of Geosciences (Beijing). Published thesis.
- Zorin YA** (1999) Geodynamics of the western part of the Mongolia-Okhotsk collisional belt, Trans-Baikal region (Russia) and Mongolia. *Tectonophysics* **306**, 33–56.